



Cation doped cerium oxynitride with anion vacancies for Fe-based catalyst with improved activity and oxygenate tolerance for efficient synthesis of ammonia

John Humphreys^a, Rong Lan^a, Shigang Chen^a, Marc Walker^b, Yisong Han^b, Shanwen Tao^{a,c,*}

^a School of Engineering, University of Warwick, Coventry, CV4 7AL, UK

^b Department of Physics, University of Warwick, Coventry, CV4 7AL, UK

^c Department of Chemical Engineering, Monash University, Clayton, Victoria 3800, Australia

ARTICLE INFO

Keywords:

Oxynitride
Nitrogen vacancy
Ammonia synthesis
Oxygenate
Activation energy

ABSTRACT

For the first time, new Sm doped cerium oxynitrides with the formula $Ce_{1-z}Sm_zO_{2-x}N_y$ ($z \leq 0.5$) are synthesized in order to maximize the concentration of anion vacancies. Single phase Sm-doped $CeO_{2-x}N_y$ were confirmed by XRD, HRTEM and Rietveld refinement. These oxynitrides show a great promotion effect for the low-cost Fe catalyst for the ammonia synthesis. At 350 °C and 1 MPa, the activity of 80 wt% Fe- 20 wt% $Ce_{1-z}Sm_zO_{2-x}N_y$ is one of the highest reported for non-Ru catalysts for the Haber-Bosch reaction. The apparent activation energy of the 80 wt% Fe- 20 wt% $Ce_{1-z}Sm_zO_{2-x}N_y$ catalysts with $z \geq 0.3$ is around 45 kJ/mol, which is in the lowest range among all reported ammonia synthesis catalysts. Introduction of nitrogen vacancies through doping may facilitate the mobility of nitrogen vacancies. This study demonstrates doped oxynitrides with a large concentration of anion vacancies, particularly nitrogen vacancies are excellent promoters/co-catalysts for ammonia synthesis.

1. Introduction

As one of the most important inorganic chemicals, ammonia is responsible for supporting approximately 27 % of global population [1, 2]. The Haber-Bosch process for ammonia synthesis is regarded as one of the greatest inventions of the last century [1]. Since then, a great deal of effort has been made to develop new ammonia synthesis catalysts to allow the operation of the Haber-Bosch process at reduced temperature and pressure. Intensive investigations have been carried on Ru-based catalysts promoted through a variety of different support materials Ru/HT-C12A7:e⁻ [3], Ru/ Ba-Ca(NH₂)₂ [4], Ru/BaTiO_{3-x}H_x [5], Ru/TiH₂, Ru/BaTiO_{2.5}H_{0.5} [6] and Ru/BaCeO_{3-x}N_yH_z [7]. Atomically dispersed Co supported on N-doped hollow carbon spheres also exhibit excellent catalytic activity at 350 °C [8]. Novel ammonia synthesis methods including electrochemical [9,10] and photocatalytic synthesis [11] allow ammonia synthesis at ambient conditions. The promotional effects of applied electric fields to ammonia synthesis have been reported [12]. The use of single atom catalysts for electrochemical synthesis of ammonia has been investigated through density functional theory calculations [13]. Due to the high cost of Ru, large scale application is limited with around ten ammonia synthesis plants using

Ru-based catalysts globally (in which some plants are combined with Fe-catalysts too), all remaining plants use cheap fused Fe catalysts. A large Haber-Bosch ammonia synthesis plant may need 300 tons of catalyst thus cost is extremely important. Metal hydrides, oxyhydride and oxynitride hydride have been investigated as efficient promoters/supports for Ru, Ni, Fe and Co-based catalysts [5,7,14,15]. In general, metal hydrides are sensitive to air and moisture which may limit their practical large scale applications [15,16]. In laboratory conditions, most of the electride or hydride-based catalysts are handled in a glove-box to avoid their reaction with H₂O [4–7]. In conclusion, no matter whether the catalyst is Fe/Co/Ni or Ru-based, they still fall short in terms of cost, moisture and oxygenate tolerance, therefore further improvements in this key area is still required.

In ammonia industry, whether using Fe or Ru-based catalysts, a heavy gas purification process is applied to purify the feed gases, H₂ and N₂, to avoid catalyst poisoning. Trace amounts of oxygenates (as low as 10 atomic oxygen) such as O₂, H₂O, CO, and CO₂ will deactivate the Fe-based catalyst [16–22]. In a recent report, it has been demonstrated that even impurities below 1 ppm of oxygen lead to a significant loss in activity for a state-of-the-art multi-promoted iron-based industrial catalyst [21]. A high purity gas feed of over 99.99995 % (0.5 ppm impurity), is

* Corresponding author at: School of Engineering, University of Warwick, Coventry, CV4 7AL, UK.

E-mail address: s.tao.1@warwick.ac.uk (S. Tao).

<https://doi.org/10.1016/j.apcatb.2020.119843>

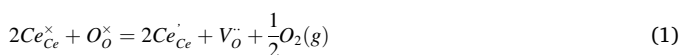
Received 6 October 2020; Received in revised form 24 November 2020; Accepted 7 December 2020

Available online 25 December 2020

0926-3373/© 2020 The Authors. Published by Elsevier B.V. This is an open access article under the CC BY license (<http://creativecommons.org/licenses/by/4.0/>).

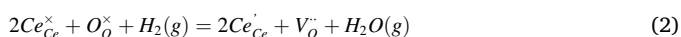
normally used in reported papers for Haber-Bosch processes [4–7]. Inevitable intensive gas purification of both H₂ and N₂ will lead to a relevant increase in capital investment on the facility as well as additional energy inputs, lowering overall efficiency. One of the strategies to improve the oxygenate tolerance of the Fe or Ru catalysts is to prevent the particle growth, under the ammonia synthesis conditions through strong metal support interaction (SMSI) [22,23]. It has been reported that the strong interaction between Ru and defects in CNTs can significantly improve the catalytic activity of Ru-based catalyst for ammonia synthesis [24].

In conventional fused Fe-based industrial catalysts, there are strong interactions between iron and the oxygen vacancies in the oxide promoters, although this intrinsic oxygen vacancy concentration is limited [18,22]. We previously reported that Ni promoted by BaZr_{0.1}Ce_{0.7}Y_{0.2}O_{3-δ} and Fe promoted by Ce_{0.8}Sm_{0.2}O_{2-δ} catalysts, display good ammonia synthesis activities due to the key role of extrinsic oxygen vacancies [22,25]. Anion vacancies, in particular nitrogen vacancy containing materials, provide the next step in this concept [26]. For the synthesis of ammonia through the Haber-Bosch process, the important role of nitrogen vacancies was also observed by Hosono and his co-workers in Fe, Co, Ru catalysts supported on Ba-CeO_{3-x}N_yH_z and Ni supported on LaN, with it found that nitrogen vacancies on LaN can efficiently bind and activate N₂ [7,27]. Using CeO₂ as an example, on heating up to high temperatures, intrinsic oxygen vacancies will be generated through the reduction of Ce⁴⁺ ions and the loss of lattice oxygen atoms.



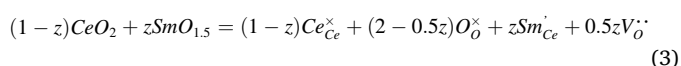
Here Kroger-Vink notations for defect chemistry is used in this article [28].

Under the ammonia synthesis conditions, due to the presence of H₂ at high temperature, some CeO₂ will be reduced to oxygen deficient CeO_{2-δ} thus forming more oxygen vacancies.



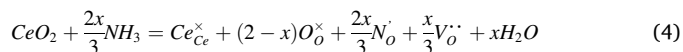
These oxygen vacancies will be a kind of nest, able to form strong interactions with the Fe or other transition metal atoms via SMSI, similar to the case for the Ag - CeO₂ system [22,23,29]. Similarly, Goula et al. reported excellent catalytic activity and stability for Ni supported on Sm₂O₃, Pr₂O₃ and MgO promoted (doped) CeO₂, attributed to the high concentration of oxygen vacancies [30].

Oxygen vacancies introduced through thermal treatment or reduction are referred to as intrinsic oxygen vacancies. Their concentration is greatly related to temperature and oxygen partial pressure. If the promotion effects were solely related to intrinsic oxygen vacancies, it would be very limited. However, oxygen vacancies can be deliberately introduced into oxides through doping with another metal oxide with lower metal valence than the parent oxides theoretically existing in any temperature range, provided a stable solid solution is formed. These oxygen vacancies are referred to as extrinsic oxygen vacancies. The concentration of oxygen vacancies can be controlled through adjusting the doping level within the solid solution limit while more oxygen vacancies will be generated at higher doping levels. This technology is used for solid oxide fuel cells (SOFCs) and other electrochemical devices. For example, Sm₂O₃ can be used to dope CeO₂, generating extrinsic oxygen vacancies,



In order to maximize the concentration of oxygen vacancies, doping the oxygen with another more negatively charged anion, such as N³⁻ ions is another option. It has been reported that when firing a porous CeO₂ membrane in NH₃ at 550 °C, N-doped CeO₂ i.e. CeO_{2-x}N_y was formed, with x = 0.1 [31]. During the activation of the ammonia synthesis catalysts in mixed N₂ and H₂, it is inevitable that ammonia will be

generated, further reacting with CeO₂ or doped CeO₂ to form N-doped CeO₂, as shown in the reaction below.



When Sm-doped CeO₂, Ce_{1-z}Sm_zO_{2-δ}, is exposed to NH₃ at high temperature, cation Sm³⁺ and anion N³⁻ co-doped CeO₂, Ce_{1-z}Sm_zO_{2-x}N_y, oxynitrides will be formed which have a higher concentration of oxygen/anion vacancies. Due to the second type of anions, N³⁻ ions, the vacancies are more precisely described as anion vacancies, which could be either oxygen vacancies, V_o[·] or/and nitrogen vacancies, V_N[·]. Fig. 1 shows the diagram to maximize the anion vacancies in CeO₂ through both cation and anion co-doping. From the charge balance, more anion vacancies will be generated when some O²⁻ ions are further replaced by lower valence ions such as N³⁻ ions. Co-doping of Sm³⁺ and N³⁻ ions in CeO₂ will maximise the generation of extrinsic anion vacancies. It is anticipated that a significantly greater promotion effects can be achieved by using materials with more tailorable extrinsic anion vacancies such as Sm-doped cerium oxynitrides, Ce_{1-z}Sm_zO_{2-x}N_y. At high anion vacancy concentrations the interaction between the positively charged anion vacancies and the electron-rich metal particles will be stronger, adding to an already strong SMSI, the nested or anchored metal particles on the anion vacancies will inhibit sintering and growth, improving metal catalyst stability [22,32–34].

Another poisoning mechanism of oxygenates is the competitive adsorption between oxygen and nitrogen on the catalyst surface, with oxygen occupying active sites limiting catalytic activity [17]. The presence of large amounts of extrinsic anion vacancies on the surface of Sm-doped cerium oxynitrides will provide more active sites (anion vacancies) available for the adsorption of oxygenates such as O₂, and H₂O, reducing poisoning severity on the metal catalyst while retaining high activity even at high concentrations of oxygenate impurities. CeO₂-based oxides have been reported as excellent oxygen storage materials for efficient catalytical conversion of H₂, CO, CO₂ and hydrocarbons [35–38].

Nitrogen is larger than oxygen, no matter in atomic or ionic format. At a coordination number of 4 (CN = 4), the environment of anions in fluorite structure, the ionic size of O²⁻ and N³⁻ ions is 1.38 and 1.46 Å respectively [39]. Thus, the size of the nitrogen atom in N₂ may match better with nitrogen vacancies than oxygen vacancies, introducing extra nitrogen vacancies may further improve the promotion effect for efficient synthesis of ammonia through the Haber-Bosch process. Therefore, in this study, Sm³⁺ and N³⁻ co-doped CeO₂, Sm-doped cerium oxynitrides (Ce_{1-z}Sm_zO_{2-x}N_y) with z ≤ 0.5 were synthesized and their promotion effects on ammonia synthesis were investigated in detail. The Ce_{1-z}Sm_zO_{2-x}N_y promoter was synthesized in a simple one-step combustion synthesis method carried out in air. It is found that both the stability and catalytic activity of iron based catalysts have been improved by deliberately introducing extrinsic anion (oxygen and nitrogen) vacancies into the Ce_{1-z}Sm_zO_{2-x}N_y promoter/co-catalyst.

2. Experimental

2.1. Materials synthesis

CeO_{2-x}N_y was prepared from a mixture of Ce(NO₃)₃·6H₂O (99.5 % Alfa Aesar) and urea with a mole ratio of 1 to 10 respectively [40]. 50 mL of water was then added to the mixture in a ceramic evaporating dish. The mixture was then treated at 120 °C for 24 h to form a gel like product which was combusted at 400 °C to form the desired CeO_{2-x}N_y powder. Part of this sample was then further calcined at 550 °C for 3 h in air to form the calcined CeO_{2-x}N_y powder. The resulting CeO_{2-x}N_y powder was then mechanically mixed with Fe₂O₃ and reduced using the same method previously reported [22].

The solubility limit of Sm₂O₃ in Ce_{1-z}Sm_zO_{2-δ} is roughly at z = 0.5 [41]. The CeO_{2-x}N_y and Ce_{1-z}Sm_zO_{2-x}N_y with z ≤ 0.5 were synthesised

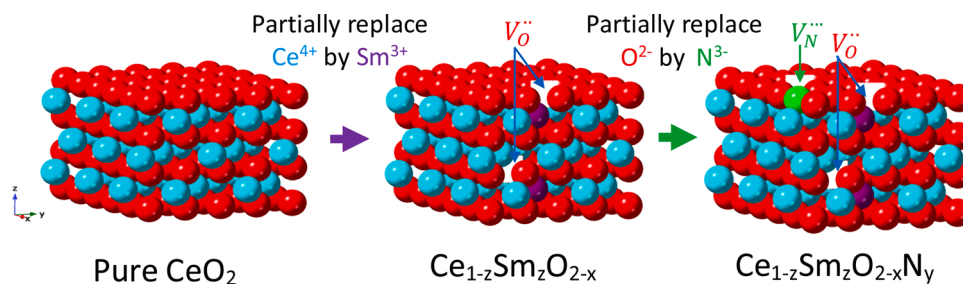


Fig. 1. Schematic diagram for the anion vacancy formation in Sm- and N- co-doped CeO_2 .

from cerium nitrate, samarium nitrate and urea through a simple combustion method [40]. $\text{Ce}_{1-z}\text{Sm}_z\text{O}_{2-x}\text{N}_y$ was prepared from a mixture of $\text{Ce}(\text{NO}_3)_3 \cdot 6\text{H}_2\text{O}$ (99.5 % Alfa Aesar), $\text{Sm}(\text{NO}_3)_3 \cdot 6\text{H}_2\text{O}$ (99.9 % Alfa Aesar), and urea with a ratio of 1 mole of total metal ions to 10 mole of urea. The rest of the synthesis process was the same as described above for $\text{CeO}_{2-x}\text{N}_y$ and was repeated for z values of 0.1, 0.2, 0.3, 0.4, and 0.5. The rest is the same as for preparation of $\text{CeO}_{2-x}\text{N}_y$. The combustion method was used to prepare pure CeO_2 as previously reported [22].

2.2. Materials characterisation

Before materials characterisation, all samples were washed multiple times by water and ethanol to remove any residual urea or other hydrocarbons. The catalyst was characterised using X-ray Diffraction (XRD), X-ray photoelectron spectroscopy (XPS), Carbon, Hydrogen and Nitrogen (CHN), Raman spectroscopy, Scanning electron microscopy (SEM) and high resolution transmission electron microscopy (HRTEM). XRD analyses were carried out on a Panalytical X'Pert Pro Multi-Purpose Diffractometer (MPD), with Cu K α 1 radiation, working at 45 kV and 40 mA. The nitrogen content was measured by a CHN analysis, performed on a FlashEA® 1112 Element Analyzer at MEDAC Ltd adhering to UKAS ISO17025 accreditation, with a standard deviation of ± 0.3 wt%. The same CHN facility has previously been used to determine the nitrogen content in ammonia synthesis catalyst $(\text{Ni},\text{M})_2\text{Mo}_3\text{N}$ ($\text{M} = \text{Cu}$ or Fe) [42]. The SEM images were obtained with ZEISS SUPRA 55-VP operating at 10 kV. Elemental compositions were analysed with an energy-dispersive X-ray spectrometer (EDX) attached to the SEM. X-ray Photoelectron Spectroscopy (XPS) data were collected at the Warwick Photoemission Facility, University of Warwick. Samples were attached to electrically conductive carbon tape and mounted on a sample bar loaded in to a Kratos Axis Ultra DLD spectrometer (base pressure $< 2 \times 10^{-10}$ mbar). Samples were illuminated using a monochromated Al K α X-ray source ($h\nu = 1486.7$ eV). The core level spectra were recorded using a pass energy of 20 eV (resolution approx. 0.4 eV), from an analysis area of $300 \mu\text{m} \times 700 \mu\text{m}$. The data were analysed in the CasaXPS package, using Shirley backgrounds and mixed Gaussian-Lorentzian (Voigt) lineshapes. High resolution transmission electron microscopy (HRTEM) observations of the samples were carried out on a JEOL2100 microscope, operated at 200 kV, equipped with an Oxford Instruments 80 mm^2 SDD EDX detector. EDX spectra were collected by focusing the electron beam onto a certain area of the samples.

2.3. Measurements of catalytic activities

To measure the catalytic activity, a fixed bed stainless steel reactor was used with the catalyst held in place in the centre by quartz granules and glass fibre. The total weight after activation / reduction was approximately 0.3 g for each catalyst tested. Full details on the testing parameters used along with the gas purification process can be found in our previous report [22]. The data points in Fig. 9 were obtained through the purification and known impurity injection process detailed in our previous work [22].

Produced ammonia was collected in dilute sulfuric acid (0.01 M) with concentration measured using an ISE Thermo Scientific Orion Star A214 ammonia meter [25]. The rate of ammonia production (in $\text{mol g}^{-1} \text{h}^{-1}$) was calculated according to the following equation.

$$r_{\text{NH}_3} = \frac{[\text{NH}_4^+] \times V}{t \times m} \quad (5)$$

Where $[\text{NH}_4^+]$ is ammonia concentration in mol L^{-1} , V is volume of 0.01 M H_2SO_4 in L, t is time in hours and m is catalyst mass in g.

3. Results

3.1. Structure and composition of new Sm-doped cerium oxynitrides

3.1.1. CHN analysis to determine the nitrogen content

Carbon, Hydrogen and Nitrogen (CHN) analysis was carried out to precisely measure the overall nitrogen content in the synthesised oxynitrides. In our synthesis process of cerium oxynitride, urea was used as the nitrogen source. It is believed that, during the combustion process, ammonia is generated from urea to further react with CeO_2 to form cerium oxynitride, $\text{CeO}_{2-x}\text{N}_y$. Assuming the charge for cerium is +4, from the charge balance, the formula of the cerium oxynitride can be written as $\text{CeO}_{2-x}\text{N}_{\frac{2x}{3}}\text{V}_{\frac{x}{3}}$, where 'V' represents anion vacancies, oxygen or/and nitrogen vacancies. For Sm-doped cerium oxynitrides, the general formula can be written as $\text{Ce}_{1-z}\text{Sm}_z\text{O}_{2-\frac{y+z}{2}}\text{N}_y\text{V}_{\frac{3y+z}{2}}$. As z is known from the starting materials, and since the weight percentage of nitrogen in the synthesised oxynitrides is measured, y can be then deduced. Therefore, the general formulae of these new oxynitrides can be determined based on the nitrogen content, which are listed in Table 1. For samples with $z = 0$ and 0.1, the nitrogen content is $y = 0.07$ for anion sites for both samples (Table 1). However, the anion vacancy concentration for the Sm-doped sample, $\text{Ce}_{0.9}\text{Sm}_{0.1}\text{O}_{1.84}\text{N}_{0.07}$, is 4.5 %, which is slightly higher than that of the Sm-free sample, $\text{CeO}_{1.89}\text{N}_{0.07}$ (3.5 %). This is due

Table 1

The composition of different samples derived from the nitrogen content measured by CHN and XPS analyses and the derived percentage of anion vacancies.

Sample	N content results from CHN (wt%)	Derived chemical composition	Anion vacancy (% of unoccupied anion sites)
$\text{CeO}_{2-x}\text{N}_y$	0.59	$\text{CeO}_{1.89}\text{N}_{0.07}$	3.5
$\text{Ce}_{0.9}\text{Sm}_{0.1}\text{O}_{2-x}\text{N}_y$	0.59	$\text{Ce}_{0.9}\text{Sm}_{0.1}\text{O}_{1.84}\text{N}_{0.07}$	4.5
$\text{Ce}_{0.8}\text{Sm}_{0.2}\text{O}_{2-x}\text{N}_y$	0.63	$\text{Ce}_{0.8}\text{Sm}_{0.2}\text{O}_{1.78}\text{N}_{0.08}$	7
$\text{Ce}_{0.7}\text{Sm}_{0.3}\text{O}_{2-x}\text{N}_y$	1.01	$\text{Ce}_{0.7}\text{Sm}_{0.3}\text{O}_{1.66}\text{N}_{0.12}$	11
$\text{Ce}_{0.6}\text{Sm}_{0.4}\text{O}_{2-x}\text{N}_y$	1.52	$\text{Ce}_{0.6}\text{Sm}_{0.4}\text{O}_{1.52}\text{N}_{0.19}$	14.5
$\text{Ce}_{0.5}\text{Sm}_{0.5}\text{O}_{2-x}\text{N}_y$	1.29	$\text{Ce}_{0.5}\text{Sm}_{0.5}\text{O}_{1.51}\text{N}_{0.16}$	16.5
$\text{Ce}_{0.5}\text{Sm}_{0.5}\text{O}_{2-x}\text{N}_y$	4.67 at% from XPS	$\text{Ce}_{0.5}\text{Sm}_{0.5}\text{O}_{1.45}\text{N}_{0.12}$	16.5

to the doping of low valent Sm^{3+} cations in the $\text{Ce}_{0.9}\text{Sm}_{0.1}\text{O}_{1.84}\text{N}_{0.07}$ sample, thus more anion vacancies are generated (Fig. 1, eq. 3). According to the data in Table 1, in general, the nitrogen content and anion vacancies increase with increased Sm-doping level. The only exceptional situation is that, the nitrogen content in sample $\text{Ce}_{0.5}\text{Sm}_{0.5}\text{O}_{1.51}\text{N}_{0.16}$ is slightly lower than that for sample $\text{Ce}_{0.6}\text{Sm}_{0.4}\text{O}_{1.52}\text{N}_{0.19}$. The possible reason is, at $z = 0.5$, the cation doping level is already very high leading to a high concentration of anion vacancies. If more oxygen is replaced by nitrogen, more anion vacancies will be generated. However, there is a limit on the anion vacancy concentration in the oxynitride in order to maintain the crystal lattice. Under this circumstance the nitrogen content is slightly reduced for the sample $\text{Ce}_{0.5}\text{Sm}_{0.5}\text{O}_{1.51}\text{N}_{0.16}$. For representative sample $\text{Ce}_{0.5}\text{Sm}_{0.5}\text{O}_{2-x}\text{N}_y$, the compositions were also estimated using X-ray Photoelectron Spectroscopy (XPS).

3.1.2. XPS analysis of the samples

Fig. 2 shows the selected XPS data for pure $\text{Ce}_{0.5}\text{Sm}_{0.5}\text{O}_{2-x}\text{N}_y$ promoter plus the $\text{Ce}_{0.5}\text{Sm}_{0.5}\text{O}_{2-x}\text{N}_y$ promoter with Fe_2O_3 and Fe before and after the activity test. For the pure oxynitride, XPS revealed a composition of $\text{Ce}_{0.5}\text{Sm}_{0.5}\text{O}_{1.45}\text{N}_{0.12}$, a slightly lower nitrogen content than that derived from the CHN results. The ratio of Ce(IV) to Ce(III) was found to be 3.8, with a corresponding ratio of Sm(III) to Sm(II) of 2.6, the XPS spectrum of Ce 3d and Sm 3d are shown in Figure S1. Analysis of the N 1s spectrum acquired from the $\text{Ce}_{0.5}\text{Sm}_{0.5}\text{O}_{2-x}\text{N}_y$ sample is shown in Fig. 2b and corresponds to a nitrogen content of 4.67 at% (Table 1). The N 1s spectrum is further shown in Figure S1c, showing large deviation in the exp count values. This indicates that the nature of the nitrogen bonds obtained from the XPS spectra is unreliable with the main conclusion being the presence of nitrogen. The C 1s spectrum is shown in Figure S1d showing no C—N bonds confirming no residual urea present in the sample. The discrepancy in nitrogen content derived from XPS and CHN is due to the surface specificity of XPS. While CHN measures the overall nitrogen content, the sampling depth in XPS is limited to the outermost few nm of the material and thus a little deviation is common. The deduced overall unoccupied anion sites, i.e., the total anionic vacancies is the same (16.5 %), due to the detection of Ce(III) and Sm(II) in the XPS results, allowing us to remove the assumption that all cerium has a charge of +4 and all Sm has a charge of +3 (Table S1).

The compositions of the Fe_2O_3 and Fe promoted catalysts are less reliable with Ce to Sm ratio varying drastically from the expected value. This is due to the overlap between Ce 3d and the Fe Auger emission as well as Ce 4d and Sm 4d, both of which make the determination of the amount of Ce less accurate. To resolve this, a sample with low Ce content was examined in order to obtain a reliable line shape for the Fe $\text{LM}_{23}\text{M}_{23}$ Auger emission. For the two promoted catalysts, Fe_2O_3 and Fe before and after the activity test, examination of the Sm 3d region showed no Sm(II) present, with all samarium being Sm(III). Although no Sm(II) was detected on the surface in these samples it should be noted that the weight percent of oxynitride in these samples is only 20 wt%, much lower than in the pure $\text{Ce}_{0.5}\text{Sm}_{0.5}\text{O}_{2-x}\text{N}_y$ sample and therefore signal for Sm(II) could be below the detection limit. However, for the calculation of composition it was assumed that only Sm(III) was present. The ratio of Ce(IV) to Ce(III) was 0.87 and 3.7 in 85 wt% $\text{Fe}_2\text{O}_3 - 15$ wt % $\text{Ce}_{0.5}\text{Sm}_{0.5}\text{O}_{2-x}\text{N}_y$ and Fe - 20 wt % $\text{Ce}_{0.5}\text{Sm}_{0.5}\text{O}_{2-x}\text{N}_y$ respectively. This deviation from the pure oxynitride sample was expected to be due to the overlap of emission spectra as described above. For the mixed 85 wt% $\text{Fe}_2\text{O}_3 - 15$ wt % $\text{Ce}_{0.5}\text{Sm}_{0.5}\text{O}_{2-x}\text{N}_y$, the Fe spectra is shown in Fig. 2c. All Fe is in the form of Fe_2O_3 . After the catalytic activity test, the Fe spectra for the 80 wt%Fe - 20 wt % $\text{Ce}_{0.5}\text{Sm}_{0.5}\text{O}_{2-x}\text{N}_y$ catalyst is shown in Fig. 2e. 76 % of this region is made up of Fe_2O_3 which is expected due to the reoxidation of the small Fe catalyst particles upon removal of the catalyst from the reactor. 21 % of the region is Fe (II) with the remaining 3 % being zero valence Fe(0). However, after reduction and the catalytic activity test, no nitrogen is detected in the 80 wt%Fe - 20 wt % $\text{Ce}_{0.5}\text{Sm}_{0.5}\text{O}_{2-x}\text{N}_y$ sample. One possibility is the nitrogen content is too low, beyond the measuring limit of XPS. Another possible reason is, the oxynitride sample is partially oxidized by the oxygenates present in the gas stream. However, the Sm-doped CeO_2 , $\text{Ce}_{1-z}\text{Sm}_z\text{O}_{2-\delta}$, still exhibit good stability and activity for ammonia synthesis, which is related to the extrinsic oxygen vacancies, although the overall activity is slightly lower [22].

3.1.3. XRD analysis and Rietveld refinements of crystal structure

X-ray diffraction (XRD) was used to determine the phase and structure of the synthesised oxynitrides. As shown in Fig. 3a, the XRD patterns of pure and Sm-doped $\text{CeO}_{2-x}\text{N}_y$ are similar to CeO_2 , indicating

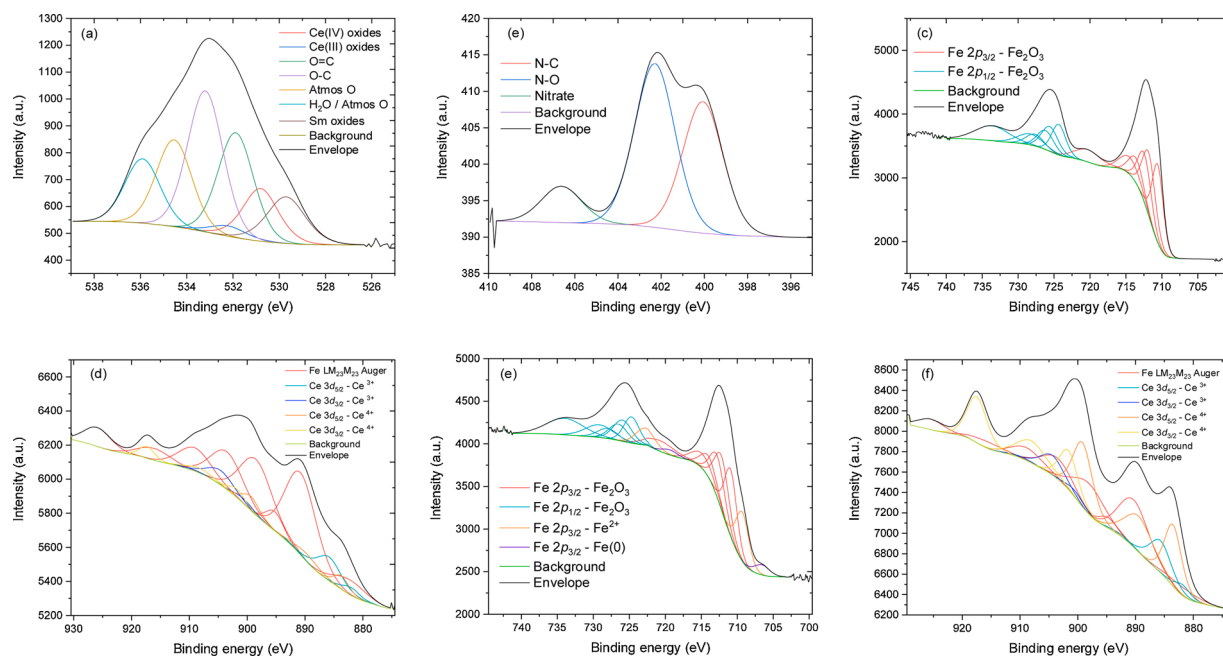


Fig. 2. XPS Spectra for key elements in pure $\text{Ce}_{0.5}\text{Sm}_{0.5}\text{O}_{2-x}\text{N}_y$, $\text{Fe}_2\text{O}_3 - 15\%$ $\text{Ce}_{0.5}\text{Sm}_{0.5}\text{O}_{2-x}\text{N}_y$ and Fe - 20% $\text{Ce}_{0.5}\text{Sm}_{0.5}\text{O}_{2-x}\text{N}_y$. (a) O 1s spectra for pure $\text{Ce}_{0.5}\text{Sm}_{0.5}\text{O}_{2-x}\text{N}_y$. (b) N 1s spectra for pure $\text{Ce}_{0.5}\text{Sm}_{0.5}\text{O}_{2-x}\text{N}_y$. (c) Fe 2p spectra for $\text{Fe}_2\text{O}_3 - 15\%$ $\text{Ce}_{0.5}\text{Sm}_{0.5}\text{O}_{2-x}\text{N}_y$. (d) Ce 3d spectra for $\text{Fe}_2\text{O}_3 - 15\%$ $\text{Ce}_{0.5}\text{Sm}_{0.5}\text{O}_{2-x}\text{N}_y$. (e) Fe 2p spectra for Fe - 20% $\text{Ce}_{0.5}\text{Sm}_{0.5}\text{O}_{2-x}\text{N}_y$. (f) Ce 3d spectra for Fe - 20% $\text{Ce}_{0.5}\text{Sm}_{0.5}\text{O}_{2-x}\text{N}_y$.

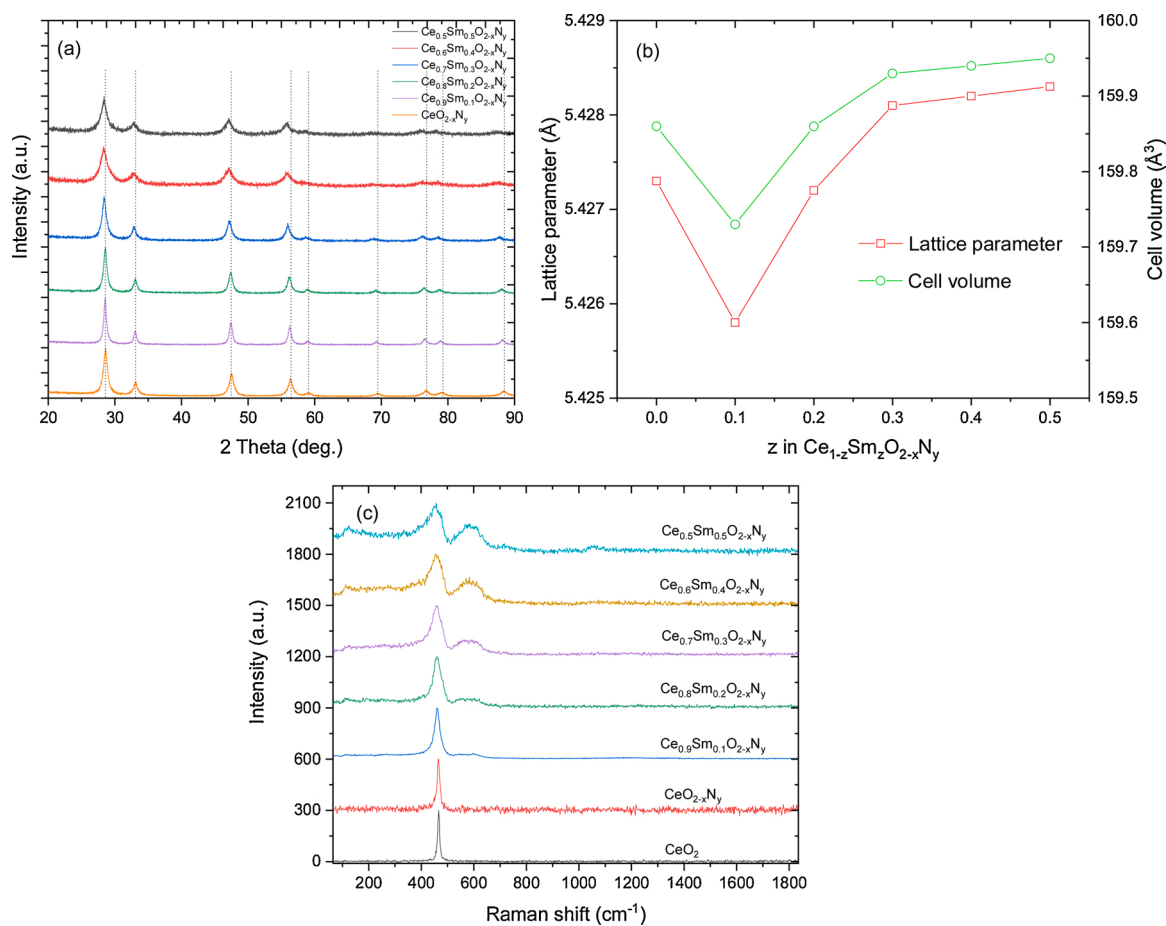


Fig. 3. (a) The room temperature XRD patterns of $Ce_{1-z}Sm_zO_{2-x}N_y$ with $z = 0.1$ to 0.5 ; (b) The refined lattice parameter and cell volume for samples $Ce_{1-z}Sm_zO_{2-x}N_y$ with z from 0 to 0.5 from GSAS; (c) The Raman spectra of pure CeO_2 , $CeO_{2-x}N_y$ and $Ce_{1-z}Sm_zO_{2-x}N_y$ with $z = 0.1$ to 0.5 .

they have the same or a similar crystal structure to CeO_2 . Rietveld refinement of these oxynitrides were carried out by GSAS + EXPGUI using the fluorite structure for pure CeO_2 as the parent phase (Figure S2) [43,44]. During the refinement, cubic CeO_2 with a space group $Fm\bar{3}m$ (225) was used as the parent phase. It was assumed that Ce and Sm share the 4a (0,0,0) sites, O and N share the 8c (1/4,1/4,1/4) sites [45]. The oxygen and nitrogen occupancies were taken from the chemical composition of these oxynitrides measured by CHN analysis because CHN can provide the overall nitrogen content while XPS can

only provide the information on the surface (Table 1). The real and calculated XRD patterns provide a good fit, indicating all these new materials are single phase. The lattice parameters, and cell volume thermal factors are listed in Table 2. The lattice parameters and cell volumes of $Ce_{1-z}Sm_zO_{2-x}N_y$ with $z = 0$ to 0.5 are also shown in Fig. 3b. It is believed that oxygen and nitrogen share the same 8c sites, ordering of nitrogen and oxygen, as has been observed in some oxynitrides, but does not happen in $Ce_{1-z}Sm_zO_{2-x}N_y$. It is then reasonably deduced that nitrogen is homogeneously distributed in the bulk, although the defect concentration including anion vacancies are normally higher on the

Table 2

Crystallographic refinement parameters of pure and Sm-doped cerium oxynitrides.

Crystallographic parameters	$CeO_{2-x}N_y$	$Ce_{0.9}Sm_{0.1}O_{2-x}N_y$	$Ce_{0.8}Sm_{0.2}O_{2-x}N_y$	$Ce_{0.7}Sm_{0.3}O_{2-x}N_y$	$Ce_{0.6}Sm_{0.4}O_{2-x}N_y$	$Ce_{0.5}Sm_{0.5}O_{2-x}N_y$
Crystal system	Cubic	Cubic	Cubic	Cubic	Cubic	Cubic
Space group	$Fm\bar{3}m$	$Fm\bar{3}m$	$Fm\bar{3}m$	$Fm\bar{3}m$	$Fm\bar{3}m$	$Fm\bar{3}m$
a (Å)	5.4273(1)	5.4258(1)	5.4272(1)	5.4281(1)	5.4282(1)	5.4283(1)
V (\AA^3)	159.87(1)	159.73(1)	159.86(1)	159.93(1)	159.94(1)	159.95(1)
Occupancy						
Ce	1	0.9	0.8	0.7	0.6	0.5
Sm	–	0.1	0.2	0.3	0.4	0.5
O	0.945	0.92	0.89	0.83	0.76	0.755
N	0.035	0.035	0.04	0.06	0.095	0.08
U_{iso} (\AA^2)						
Ce	0.023(1)	0.017(1)	0.018(1)	0.019(1)	0.020(1)	0.017(1)
Sm	–	0.017(1)	0.018(1)	0.019(1)	0.020(1)	0.017(1)
O	0.011(1)	0.014(2)	0.013(2)	0.017(2)	0.022(2)	0.022(2)
N	0.017(1)	0.014(2)	0.013(2)	0.017(2)	0.022(2)	0.022(2)
χ^2	1.512	3.595	1.422	1.377	1.417	1.440
R_{wp} (%)	11.69	9.71	9.62	8.62	8.48	8.62
R_p (%)	9.92	7.61	7.59	6.89	6.75	6.89

surface of a particle. From XPS analysis of sample $\text{Ce}_{0.5}\text{Sm}_{0.5}\text{O}_{2-x}\text{N}_y$, un-occupied anion sites is 16.5 %, which is the same as deduced from CHN analysis (Table 1). The crystal structure of $\text{Ce}_{0.5}\text{Sm}_{0.5}\text{O}_{2-x}\text{N}_y$ is also consistent with the observed d-spacing from high resolution transmission electron microscopy (HRTEM) (Fig. 4a), indicating it is correct. To the best of our knowledge, Sm-doped $\text{CeO}_{2-x}\text{N}_y$ is the first cation doped fluorite oxynitride.

It is noticed that the lattice parameter change in $\text{Ce}_{1-z}\text{Sm}_z\text{O}_{2-x}\text{N}_y$ with $z = 0$ to 0.5 does not follow the Vegard's law, i.e., the lattice parameter change should be proportional to the change of z in $\text{Ce}_{1-z}\text{Sm}_z\text{O}_{2-x}\text{N}_y$ (Fig. 3b). As $\text{Ce}_{1-z}\text{Sm}_z\text{O}_{2-x}\text{N}_y$ is both a cation (Sm^{3+}) and anion (N^{3-}) co-doped solid state solution, which is more complicated. It may not necessarily follow Vegard's law, which normally applies to only cation doped materials. According to CHN analysis, based on the contents of nitrogen, it can be deduced that the formula for $\text{Ce}_{1-z}\text{Sm}_z\text{O}_{2-x}\text{N}_y$ with $z = 0$ and 0.1 is $\text{Ce}_{0.189}\text{N}_{0.07}$ and $\text{Ce}_{0.9}\text{Sm}_{0.1}\text{O}_{1.84}\text{N}_{0.07}$ respectively (Table 1). The ionic size for Ce^{4+} and Sm^{3+} ions at coordination number of 8 (CN = 8) is 0.97 and 1.079 Å respectively [39]. Doping of CeO_2 by larger Sm^{3+} ions should lead to the lattice expansion. This has been previously observed in Sm-doped CeO_2 [46]. However, the introduction of nitrogen in the lattice makes things more complicated. The lattice parameter of the synthesized $\text{CeO}_{2-x}\text{N}_y$ is $a = 5.4273(1)$ Å. This is slightly lower than the reported $a = 5.5133(1)$ Å for pure CeO_2 [47]. The ionic size of N^{3-} ions is larger than O^{2-} ions [39]. From this point of view, partially replacing O^{2-} ions with larger N^{3-} ions in CeO_2 should lead to an increased lattice parameter. On the other hand, this anion doping also generates anion vacancies (charged voids), as shown in Eq. (4). This may result in lattice shrinking. The final lattice parameters of $\text{CeO}_{2-x}\text{N}_y$ is the combined effects of lattice expansion due to larger N^{3-} ions and lattice shrinking due to the formation of anion vacancies. Lattice shrinking was also observed in some perovskite oxynitrides where some lattice O^{2-} ions are replaced by large N^{3-} ions, which is attributed to the formation of higher valent cation ions [48]. XPS analyses indicate both Ce^{4+} and Ce^{3+} for element Ce, and Sm^{3+} and Sm^{2+} for element Sm, exist on the surface of pure $\text{Ce}_{0.5}\text{Sm}_{0.5}\text{O}_{2-x}\text{N}_y$ (Table S1), thus no higher valent cations are formed in $\text{Ce}_{0.5}\text{Sm}_{0.5}\text{O}_{2-x}\text{N}_y$. A similar situation may happen on sample $\text{Ce}_{0.9}\text{Sm}_{0.1}\text{O}_{2-x}\text{N}_y$, which means that the lattice shrinking for sample $\text{Ce}_{0.9}\text{Sm}_{0.1}\text{O}_{2-x}\text{N}_y$ is likely due to the extra anion vacancies due to the doping of more negative N^{3-} ions in the lattice (Fig. 3b). However, from $z = 0.1$ to 0.5, the lattice parameter gradually increases indicating that the effect of larger Sm^{3+} ions on the lattice parameters becomes more significant than that from anion vacancies (Fig. 3b). These results indicate that the relationship between lattice parameters and doping level in both the cation and anion-co-doped CeO_2 is very complicated, and may not necessarily follow the Vegard's law.

3.1.4. Raman analysis to further confirm the anion vacancies

To study the oxygen vacancies in the as-prepared oxynitrides, Raman spectra of these samples were collected (Fig. 3c). Pure CeO_2 , and raw $\text{CeO}_{2-x}\text{N}_y$ show a sharp F2g peak at 465 cm^{-1} , corresponding to the typical fluorite structure of CeO_2 [40,49,50]. The peak at 570 cm^{-1} is attributed to oxygen vacancies [40,50]. No peak was observed at 570 cm^{-1} for pure CeO_2 indicating that for pure CeO_2 , intrinsic oxygen vacancy concentration is not high enough to be detected by the Raman spectroscopy. The peak at 570 cm^{-1} for raw $\text{CeO}_{2-x}\text{N}_y$ and $\text{Ce}_{0.9}\text{Sm}_{0.1}\text{O}_{2-x}\text{N}_y$ is very weak, indicating a low concentration of oxygen vacancies. This peak becomes stronger with increased Sm doping level, indicating a higher concentration of oxygen vacancies. Sample $\text{Ce}_{0.5}\text{Sm}_{0.5}\text{O}_{2-x}\text{N}_y$ with the highest doping level gives the strongest peak at 570 cm^{-1} indicating the highest concentration of oxygen/nitrogen vacancies. These results are consistent with the deduced chemical formula from CHN analyses and the corresponding anion vacancy concentration (Table 1).

3.1.5. SEM/EDS and HRTEM/EDX observation of the samples

SEM imaging was employed to further examine the surface of the catalyst promoter as well as the promoted iron catalyst before and after reduction, EDS layering allowed for a clear distinction between promoter and iron catalyst to be seen, giving a further picture of how the promoter is distributed within the catalyst. The SEM/EDS images of sample $\text{CeO}_{2-x}\text{N}_y$ are shown in Figure S3. Figure S3a shows the image for $\text{CeO}_{2-x}\text{N}_y$ with EDS layering, it is observed from this images that there is a secondary particle size distribution of approximately 1–6 μm. In Figures S3b, 3c and 3d the unreduced catalyst, catalyst after carrying out the activity test, and catalyst after carrying out the stability test are shown. The size distribution of the $\text{CeO}_{2-x}\text{N}_y$ promoter does not change showing good stability throughout the reduction and reaction processes. Figure S4 shows the SEM/EDS images of sample $\text{Ce}_{0.5}\text{Sm}_{0.5}\text{O}_{2-x}\text{N}_y$ along with the unreduced $\alpha\text{-Fe}_2\text{O}_3$ - $\text{Ce}_{0.5}\text{Sm}_{0.5}\text{O}_{2-x}\text{N}_y$ promoted catalyst and the reduced catalyst after both the activity and stability test. It can be seen from Figures S4a and 4b that $\text{Ce}_{0.5}\text{Sm}_{0.5}\text{O}_{2-x}\text{N}_y$ has a similar structure to that of $\text{CeO}_{2-x}\text{N}_y$ with a secondary particle size distribution of approximately 1–10 μm. A similar particle size distribution can be seen for $\text{Ce}_{0.5}\text{Sm}_{0.5}\text{O}_{2-x}\text{N}_y$ before reduction as well as for both reduced catalysts after activity and stability tests showing good stability throughout this process, again similar to $\text{CeO}_{2-x}\text{N}_y$.

HRTEM images of the mixed 85 wt% Fe_2O_3 -15 wt% $\text{Ce}_{0.5}\text{Sm}_{0.5}\text{O}_{2-x}\text{N}_y$ catalyst before and after catalytic activity measurements are shown in Figs. 4a & 4b, respectively. In Fig. 4a, the closest match to 0.294 nm is the (111) spacing of $\text{Ce}_{0.5}\text{Sm}_{0.5}\text{O}_{2-x}\text{N}_y$ (0.3134 nm) and, for 0.482 nm it is the (003) spacing of $\alpha\text{-Fe}_2\text{O}_3$ (0.4582 nm). This indicates the crystal structure determined by Rietveld refinement for sample $\text{Ce}_{0.5}\text{Sm}_{0.5}\text{O}_{2-x}\text{N}_y$ is correct. In Fig. 4b, the closest match to 0.318 nm is $\text{Ce}_{0.5}\text{Sm}_{0.5}\text{O}_{2-x}\text{N}_y$.

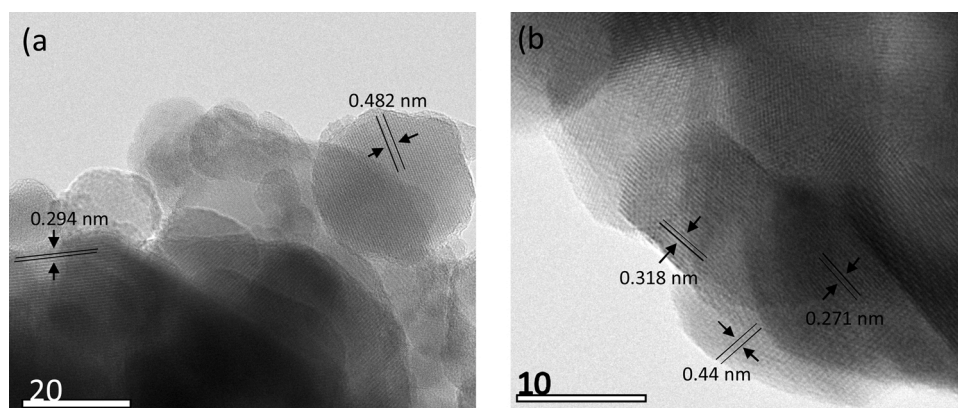


Fig. 4. (a) TEM image for 85 wt % Fe_2O_3 - 15 wt % $\text{Ce}_{0.5}\text{Sm}_{0.5}\text{O}_{2-x}\text{N}_y$ at 300k magnification (b) TEM image for 80 wt % Fe - 20 wt % $\text{Ce}_{0.5}\text{Sm}_{0.5}\text{O}_{2-x}\text{N}_y$ at 600k magnification.

xN_y (111) (0.3134 nm), for 0.271 nm it is $Ce_{0.5}Sm_{0.5}O_{2-x}N_y$ (200) (0.271 nm), and for 0.44 nm it is $\alpha-Fe_2O_3$ (100) (0.436 nm). This is consistent with the XRD pattern of the Fe- $Ce_{0.5}Sm_{0.5}O_{2-x}N_y$ catalyst after the catalytic activity measurement (Figure S5b). From XPS analyses, only 2.6at % of iron is in metallic Fe form in the sample after the catalytic measurement with the rest reoxidized by air when removed from the reactor at room temperature. Therefore it is difficult to find metallic Fe particles during TEM observations (Table S1). In Fig. 4b it can be seen that small $\alpha-Fe_2O_3$ is present on the surface of $Ce_{0.5}Sm_{0.5}O_{2-x}N_y$ particles providing indirect evidence of anchoring of Fe in $Ce_{0.5}Sm_{0.5}O_{2-x}N_y$ (or $Ce_{0.5}Sm_{0.5}O_{2,\delta}$ after oxynitride is oxidised to oxide by oxygenates) through SMSI. Iron is expected to be in the form of metallic Fe under ammonia synthesis conditions. However, when removed from the reactor the small particle size of metallic iron will cause re-oxidation, which has been confirmed by XPS analyses (Fig. 2 and Table S1). Figure S6 shows the TEM images with EDX for the 85 wt% Fe_2O_3 -15 wt% $Ce_{0.5}Sm_{0.5}O_{2-x}N_y$ catalyst before and after catalytic measurements. Before the catalytic measurement, it is a mixture of Fe_2O_3 and $Ce_{0.5}Sm_{0.5}O_{2-x}N_y$ resulting from the mechanical mixture (Figure S5b & S6a). Element nitrogen was not detected by EDX because the content is too low, beyond the measuring limit of EDX. Figure S6b shows the presence of small particle sized Fe_2O_3 on the $Ce_{0.5}Sm_{0.5}O_{2-x}N_y$ surface while a large portion of Fe or FeO_x is not in direct contact with $Ce_{0.5}Sm_{0.5}O_{2-x}N_y$ because it contains only 20 wt% in the composite.

From the analyses above, single phase doped oxynitrides, $Ce_{1-z}Sm_zO_{2-x}N_y$ with a large amount of extrinsic anion vacancies have been successfully synthesised and confirmed. They are expected to be

excellent promoters/co-catalysts for ammonia synthesis catalysts, which are investigated in detail below.

3.2. Activities of Fe- $CeO_{2-x}N_y$ composite catalysts at different mass ratio of Fe to $CeO_{2-x}N_y$

These oxynitrides were investigated as promoters with a Fe catalyst for the synthesis of ammonia. The experimental details are described in the experimental section. In our experiments it was found that, under 3 MPa, pure Fe catalyst using $\alpha-Fe_2O_3$ as the precursor, pure CeO_2 , pure Sm_2O_3 , $CeO_{2-x}N_y$ and $Ce_{0.5}Sm_{0.5}O_{2-x}N_y$ all show no activity towards ammonia synthesis on their own at temperatures up to 600 °C with feed gas purity of 99.996 %. When $\alpha-Fe_2O_3$ was mixed with $CeO_{2-x}N_y$, ammonia was successfully generated (Fig. 5a&5b). This indicates the catalytic activity is a synergetic process between the $\alpha-Fe$ catalyst and the oxynitride promoter/co-catalyst. The oxynitride may not be a simple promoter as pure Fe from reduction of $\alpha-Fe_2O_3$ itself does not show any activity. The oxynitride in the Fe-oxynitride composite is more likely a co-catalyst, which needs further investigation.

For a synergetic process, normally there is an optimised ratio between Fe and the oxynitride, which exhibits the best catalytic activity. To find an optimal ratio between the Fe catalyst and the oxynitride promoter, the weight of oxynitride promoter was varied from 14 wt% to 26 wt% in the total Fe-oxynitride composite catalysts. The catalytic activities of these Fe-based catalysts were initially measured in a fixed bed reactor using BOC Zero grade N_2 and H_2 as the feed gases without further purification. The impurity level of these gases has been listed in a

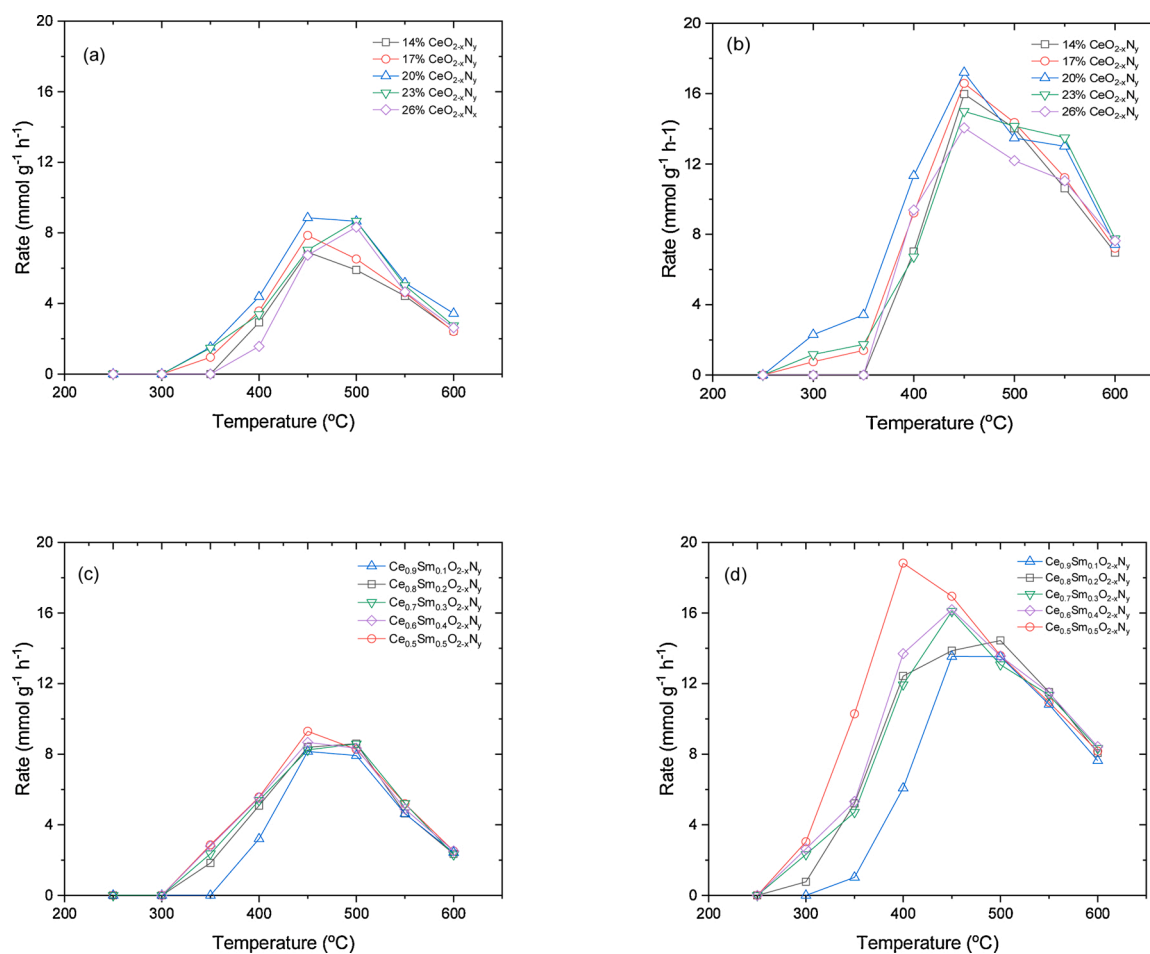


Fig. 5. Ammonia synthesis rate for (a) Fe - $CeO_{2-x}N_y$ with 14 to 26 % promoter weight percentage at 1 MPa. (b) Fe - $CeO_{2-x}N_y$ with 14 to 26 % promoter weight percentage at 3 MPa. Ammonia synthesis rate for (c) Fe - 20 % $Ce_{1-z}Sm_zO_{2-x}N_y$ with z values between 0.1 and 0.5 at 1 MPa. (d) Fe - 20 % $Ce_{1-z}Sm_zO_{2-x}N_y$ with z values between 0.1 and 0.5 at 3 MPa.

previous report [22]. Unless specified, all the activities were obtained from Zero grade feed gases.

Fig. 5a & b show the ammonia synthesis activity of $\text{CeO}_{2-x}\text{N}_y$ promoted Fe catalysts at different weight percentages over a temperature range of 600 °C - 250 °C, at 1 MPa and 3 MPa respectively. Apart from 77 % Fe - 23 % $\text{CeO}_{2-x}\text{N}_y$ and 74 % Fe - 26 % $\text{CeO}_{2-x}\text{N}_y$, both achieving their

maximum activity at 500 °C and 1 MPa, all the other experiments suggested an optimum operation temperature of 450 °C. At 3 MPa the highest activity was 17.2 $\text{mmol g}^{-1} \text{h}^{-1}$ with the optimum weight ratio of 80 % Fe - 20 % $\text{CeO}_{2-x}\text{N}_y$. At 1 MPa, the highest activity was again achieved for 80 % Fe - 20 % $\text{CeO}_{2-x}\text{N}_y$, 8.86 $\text{mmol g}^{-1} \text{h}^{-1}$. The optimum mass ratio of Fe to $\text{CeO}_{2-x}\text{N}_y$ is found to be 80:20, as could be reasonably

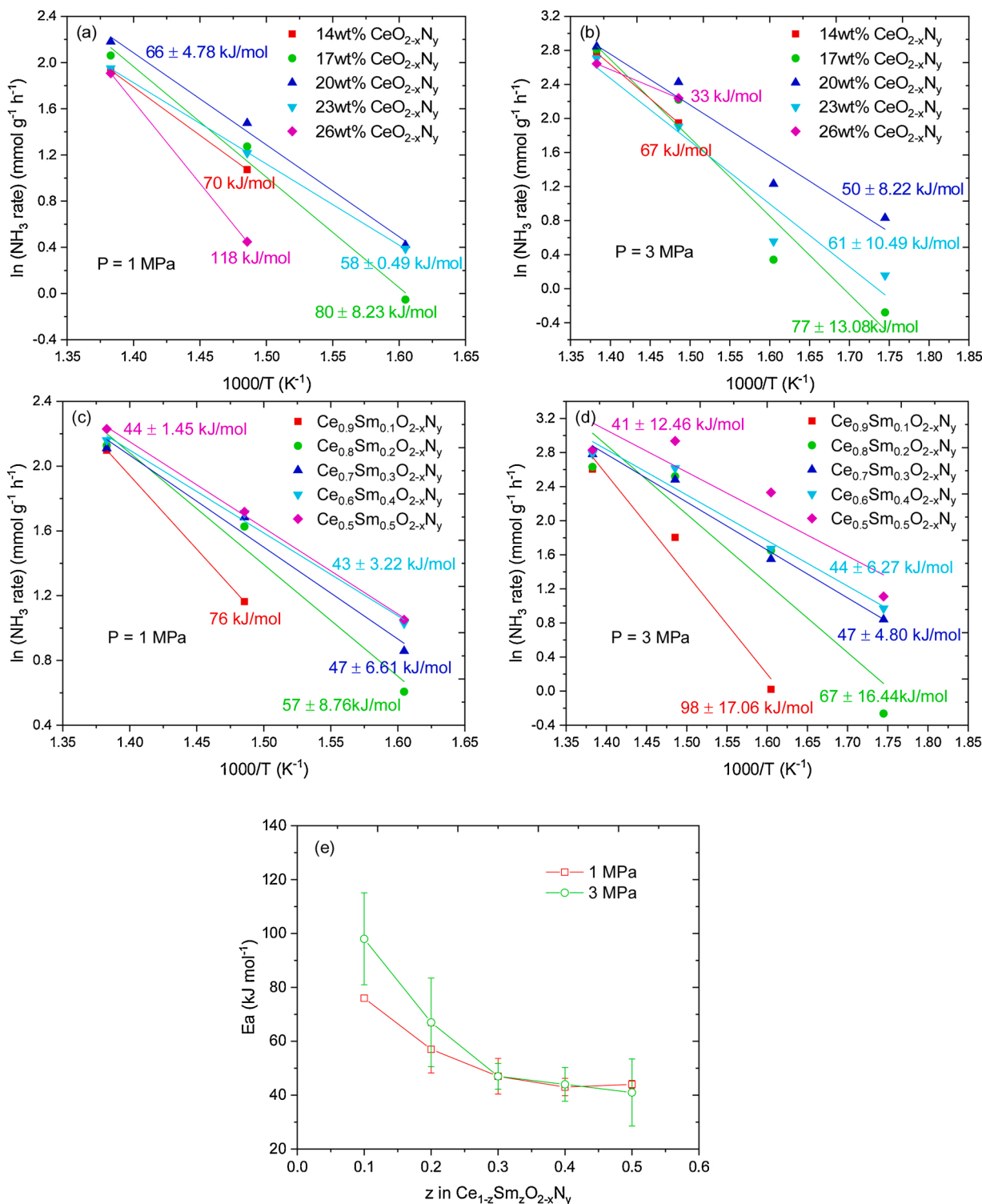


Fig. 6. Arrhenius plots used to find activation energies. (a) Fe - $\text{CeO}_{2-x}\text{N}_y$ with 14 to 26 % promoter weight percentage at 1 MPa; (b) Fe - $\text{CeO}_{2-x}\text{N}_y$ with 14 to 26 % promoter weight percentage at 3 MPa; (c) Fe - 20 % $\text{Ce}_{1-z}\text{Sm}_z\text{O}_{2-x}\text{N}_y$ with z values between 0.1 and 0.5 at 1 MPa; (d) Fe - 20 % $\text{Ce}_{1-z}\text{Sm}_z\text{O}_{2-x}\text{N}_y$ with z values between 0.1 and 0.5 at 3 MPa; (e) The apparent activation energy of the Fe- $\text{Ce}_{1-z}\text{Sm}_z\text{O}_{2-x}\text{N}_y$ catalyst for ammonia synthesis under pressure of 1 and 3 MPa respectively.

expected according to the synergetic process between Fe and oxynitride promoter. It is expected that the greater the oxynitride content then the stronger SMSI effect will be, as described above [29]. More oxynitride means more anion vacancies thus higher activity. However, the content of Fe is also important as Fe is the actual catalyst or a co-catalyst. Therefore, if Fe is diluted too much then activity will be lower. A balance between these two effects can be achieved at an oxynitride weight percent of 20 %. The SMSI between Fe and the anion vacancies and the possible in situ Ce-H species formation on the $\text{CeO}_{2-x}\text{N}_y$ surface possibly donating electrons to the nested/anchored α -Fe particle, facilitating the dissociation of $\text{N}\equiv\text{N}$ bonds, thus improving the ammonia synthesis reaction [7]. The anion vacancies in $\text{CeO}_{2-x}\text{N}_y$ may adsorb N_2 , which takes part in the ammonia synthesis process as proposed in nitride ($\text{Co}_3\text{Mo}_3\text{N}$, LaN), perovskite oxynitride hydride ($\text{BaCeO}_{3-x}\text{N}_y\text{H}_z$) catalysts [7,27,51].

The apparent activation energy (E_a) of the Fe- $\text{CeO}_{2-x}\text{N}_y$ composite catalysts at a temperature below 450 °C is obtained from the slope when plotting the logarithm of the ammonia synthesis rate vs. $1000/T$ (Fig. 6a & b) [5,6]. At a temperature above 450 °C, limited by the thermodynamic equilibrium and the greater thermal decomposition of ammonia, the activity of Fe-based catalyst normally starts to decrease at a temperature between 450 – 500 °C [4]. Due to limited data-points at low temperature, some of the obtained apparent activation energies may have a relatively large deviation. Considering the E_a for different compositions at both 1 MPa and 3 MPa, the 80 wt% Fe-20 wt% $\text{CeO}_{2-x}\text{N}_y$ composite catalyst tends to have low apparent activation energy and high activity (Figs. 6a & b). The E_a for 80 wt% Fe-20 wt% $\text{CeO}_{2-x}\text{N}_y$ composite catalyst is 66 ± 4.78 and 50 ± 8.22 kJ/mol at 1 MPa and 3 MPa respectively. This is comparable to the E_a of 70 kJ/mol for fused industrial Fe-catalyst (Haldor Topsoe KM1) at low pressure [5,52]. For ammonia synthesis catalysts using excellent promoters, a low apparent activity energy around 50 kJ/mol is normally observed [5,7,14,27,53]. As the 80 wt% Fe catalyst in the Fe- $\text{CeO}_{2-x}\text{N}_y$ composites exhibits the optimum highest activity, the mass ratio between Fe and oxynitride is fixed to 80:20 in the composite catalysts in the following study.

3.3. Activities of 80 wt%Fe-20 wt% $\text{Ce}_{1-z}\text{Sm}_z\text{O}_{2-x}\text{N}_y$ composite catalysts at $z = 0.1$ to 0.5

From previous reports and the analyses above, anion vacancies play a crucial role in the stability and catalytic activity of ammonia synthesis catalysts. To further increase anion vacancies, new Sm-doped cerium oxynitrides of $\text{Ce}_{1-z}\text{Sm}_z\text{O}_{2-x}\text{N}_y$ with $z = 0.1$ to 0.5 were synthesised. Catalytic activity of the Fe- $\text{Ce}_{1-z}\text{Sm}_z\text{O}_{2-x}\text{N}_y$ composite catalysts with mass ratio of Fe-catalyst to $\text{Ce}_{1-z}\text{Sm}_z\text{O}_{2-x}\text{N}_y$ of 80:20 at different temperatures and pressures, 1 MPa, 3 MPa were investigated respectively (Fig. 5c & d). At both 1 MPa and 3 MPa, the sample 80 wt%Fe-20 wt% $\text{Ce}_{0.5}\text{Sm}_{0.5}\text{O}_{2-x}\text{N}_y$ where $z = 0.5$ achieved the highest activity. The introduction of samarium into the $\text{CeO}_{2-x}\text{N}_y$ promoter/co-catalyst will create extrinsic anion vacancies, confirmed by Raman spectra (Fig. 3c). From CHN analyses, nitrogen content in $\text{Ce}_{1-z}\text{Sm}_z\text{O}_{2-x}\text{N}_y$ where $x > 0.2$ is significantly higher than in the other samples, indicating the introduction of appropriate amounts of Sm^{3+} ions in CeO_2 also facilitate the incorporation of nitrogen into the lattice (Table 1). According to Eq. (4), the concentration of negatively charged nitrogen defects N'_0 will also be higher in samples with high nitrogen content. These negatively charged nitrogen defects, similar to negatively charged H^- ions, theoretically may donate electrons to nearby Fe particles, helping in the dissociation of strong $\text{N}\equiv\text{N}$ bonds, thereby leading to higher activities. At 3 MPa, the optimum temperature at which the highest activity was achieved was 500 °C for Fe- $\text{Ce}_{0.8}\text{Sm}_{0.2}\text{O}_{2-x}\text{N}_y$, 400 °C for Fe- $\text{Ce}_{0.5}\text{Sm}_{0.5}\text{O}_{2-x}\text{N}_y$, and 450 °C for the other $\text{Ce}_{1-z}\text{Sm}_z\text{O}_{2-x}\text{N}_y$ promoted Fe-catalysts (Fig. 5c & d). The optimum temperature of Fe- $\text{Ce}_{0.5}\text{Sm}_{0.5}\text{O}_{2-x}\text{N}_y$ is similar to the expensive Ru-based catalysts [16]. It is noted that sample $\text{Ce}_{0.5}\text{Sm}_{0.5}\text{O}_{2-x}\text{N}_y$ has the highest concentration of anion vacancies, which could be related to the

lower optimum operating temperature. At 1 MPa the difference in activities is much less, although the highest activity was still obtained for the Fe- $\text{Ce}_{0.5}\text{Sm}_{0.5}\text{O}_{2-x}\text{N}_y$ catalyst. At 3 MPa the highest activity of 18.8 $\text{mmol g}^{-1} \text{h}^{-1}$ at 400 °C was obtained from the 80 % Fe – 20 % $\text{Ce}_{0.5}\text{Sm}_{0.5}\text{O}_{2-x}\text{N}_y$ catalyst. The weight hourly space velocity (WHSV) is 16000 $\text{mL g}^{-1} \text{h}^{-1}$, which is less than half of those in most of the reported papers (Table S2). This low WHSV is a result of the high catalyst loading (300 mg vs 100 mg) and larger reactor (external diameter of 1/2 inch instead of 3/8 inch), compared to other research groups [5–7]. Considering the WHSV, at 400 °C, 1 MPa, the 80 wt%Fe-20 wt% $\text{Ce}_{0.5}\text{Sm}_{0.5}\text{O}_{2-x}\text{N}_y$ composite catalyst exhibits an activity (5.6 $\text{mmol g}^{-1} \text{h}^{-1}$ at 16000 $\text{mL g}^{-1} \text{h}^{-1}$) comparable to the best industrial benchmark Wüstite fused Fe catalyst (13.9 $\text{mmol g}^{-1} \text{h}^{-1}$ at 36000 $\text{mL g}^{-1} \text{h}^{-1}$, 400 °C, 0.9 MPa). However, purity of feed gas in this study is only 99.996 %, much lower than the 99.9999 % and 99.99995 % used in previous reports (Table S2).

In the Haber-Bosch process, conversion and ammonia yield are limited by thermodynamic equilibrium at high temperatures as the reaction is exothermic [54]. Therefore, synthesis of ammonia at reduced temperature will have higher conversion and reduced energy consumption. At 1 MPa and 350 °C, the activity of 80 % Fe – 20 % $\text{Ce}_{0.5}\text{Sm}_{0.5}\text{O}_{2-x}\text{N}_y$ is 2.86 $\text{mmol g}^{-1} \text{h}^{-1}$ at WHSV of 16000 $\text{ml g}^{-1} \text{h}^{-1}$, comparable to Fe-LiH (11 $\text{mmol g}^{-1} \text{h}^{-1}$ at WHSV of 60000 $\text{ml g}^{-1} \text{h}^{-1}$ [14], Ni-LaN (5.2 $\text{mmol g}^{-1} \text{h}^{-1}$ at WHSV of 36000 $\text{ml g}^{-1} \text{h}^{-1}$, 0.9 MPa) [29] (Table S2). At 350 °C, the activity of our Fe- $\text{Ce}_{0.5}\text{Sm}_{0.5}\text{O}_{2-x}\text{N}_y$ is among the highest for all reported non-Ru catalysts for the Haber-Bosch reaction despite lower feed gas purity (99.996 %) (Table S2). The loading of cheap Fe (80 wt%) in our composite catalysts is much higher than the 0.4 wt% and 1.2 wt% Fe in the $\text{BaTiO}_{2.4}\text{H}_{0.6}$ and $\text{BaCeO}_{3-x}\text{N}_y\text{H}_z$ supported catalysts making direct comparisons less meaningful. To some extent, they are different catalyst types as our oxynitride promoted Fe catalyst is closer to the industrial fused Fe catalysts which normally contain over 90 wt% Fe. It is estimated that the cost of our 80 wt%Fe-20 wt% $\text{Ce}_{0.5}\text{Sm}_{0.5}\text{O}_{2-x}\text{N}_y$ catalyst would be much lower than the LiH, $\text{BaTiO}_{2.4}\text{H}_{0.6}$, $\text{BaCeO}_{3-x}\text{N}_y\text{H}_z$ or LaN supported catalysts as cheap iron makes up the majority of the composition in our catalysts. Those with only a few weight percentage of transition metal such as Ru, Fe, Co, Ni are typically supported catalysts. The Fe-oxynitrides with 80 wt% Fe should be classified as composite catalysts.

3.4. The apparent activation energy of 80 wt%Fe-20 wt% $\text{Ce}_{1-z}\text{Sm}_z\text{O}_{2-x}\text{N}_y$ composite catalysts

The apparent activation energy for the 80 wt%Fe – 20 wt% $\text{Ce}_{1-z}\text{Sm}_z\text{O}_{2-x}\text{N}_y$ catalysts with $z = 0.1$ to 0.5 at 1 MPa and 3 MPa are also obtained through the Arrhenius plots using the activity data at a temperature below 450 °C (Fig. 6c & d). With increased z in the Sm-doped cerium oxynitrides, the E_a tends to decrease. This tendency is quite clear when the E_a is plotted against z in $\text{Ce}_{1-z}\text{Sm}_z\text{O}_{2-x}\text{N}_y$ (Fig. 6e). For $z = 0.1$, at 1 MPa, the E_a is 76 kJ/mol, which is comparable to the 70 kJ/mol at 1 MPa representative industrial KM1 catalysts [5,52]. However, when the pressure is increased to 3 MPa, E_a is also increased from 76 to 98 kJ/mol. This is common as E_a for industrial fused Fe catalyst increased to 180 kJ/mol at 10 MPa [5,55]. When $z \geq 0.2$, either at 1 MPa or 3 MPa, the E_a for all the Fe- $\text{Ce}_{1-z}\text{Sm}_z\text{O}_{2-x}\text{N}_y$ composite catalysts is lower than the E_a of 70 kJ/mol for the industrial Fe catalyst. When $z \geq 0.3$, the E_a is in the range of 45 kJ/mol and is less sensitive to pressure change from 1 to 3 MPa. The E_a for sample Fe- $\text{Ce}_{1-z}\text{Sm}_z\text{O}_{2-x}\text{N}_y$ is 43 ± 3.22 kJ mol^{-1} at 1 MPa, 44 ± 6.27 kJ mol^{-1} at 3 MPa, around 45 kJ mol^{-1} (Fig. 6e). This is comparable with the lowest E_a in reported papers for promoters/co-catalysts such as Ru/C12A7:e (49 kJ/mol at 0.1 MPa) [5, 53], Fe/LiH (46.5 kJ/mol at 1 MPa) [5,14], Fe/ $\text{BaCeO}_{3-x}\text{N}_y\text{H}_z$ (46 kJ/mol at 0.9 MPa) [7], Fe/ $\text{BaTiO}_{2.4}\text{H}_{0.6}$ (63 kJ/mol at 4 MPa) [5] and Ni-LaN (57.5 kJ/mol at 0.9 MPa) [27]. The low apparent activation energy of our Fe- $\text{Ce}_{1-z}\text{Sm}_z\text{O}_{2-x}\text{N}_y$ composite catalyst with $z \geq 0.3$ is clearly related to the high concentration of anion vacancies. The doping of large Sm^{3+} ions and introduction of nitrogen vacancies through

partial replacement of lattice oxygen by the larger nitrogen ions, leads to a lattice expansion (Fig. 3b). Please note the lattice parameters for $Ce_{1-z}Sm_zO_{2-x}N_y$ with $z \geq 0.3$ ($a \geq 5.4281(1) \text{ \AA}$) are much larger than that for sample $CeO_{2-x}N_y$ ($a = 5.4273(1) \text{ \AA}$) (Table 2, Fig. 3b). Larger lattice parameters means the void (free volume) for mobile anions vacancies is also bigger, making the possible adsorption of large N_2 molecular easier if the nitrogen vacancies take part in the ammonia synthesis reaction, as is the case for perovskite oxynitride hydride $BaCeO_{3-x}N_yH_z$ and LaN [7, 27]. A large lattice parameter will lead to high mobility of anions, which also benefits the reaction. This will be discussed later.

3.5. The relationship between activity and lattice parameters for $Ce_{1-z}Sm_zO_{2-x}N_y$

In order to figure out the relationship between lattice volume and the ammonia synthesis activity, the activity of the 80 wt%Fe-20 wt% $Ce_{1-z}Sm_zO_{2-x}N_y$ composite catalysts at different temperatures are plotted against the z values in the $Ce_{1-z}Sm_zO_{2-x}N_y$ (Fig. 7). For both 1 MPa and 3 MPa, at different temperatures, the lowest ammonia synthesis rate was observed for the Fe - $Ce_{0.9}Sm_{0.1}O_{2-x}N_y$ catalyst. This is consistent with the relatively small lattice parameters (cell volume) for $Ce_{1-z}Sm_zO_{2-x}N_y$ samples (Fig. 3b). Comparing the nitrogen content and anion vacancy concentration for samples $CeO_{2-x}N_y$ and $Ce_{0.9}Sm_{0.1}O_{2-x}N_y$, they have the same level of nitrogen content ($y = 0.07$) (Table 1), while the anion concentration in sample $Ce_{0.9}Sm_{0.1}O_{2-x}N_y$ is higher than that for $CeO_{2-x}N_y$ due to the doping of low-valent element Sm. However, the activity of Fe- $Ce_{0.9}Sm_{0.1}O_{2-x}N_y$ is lower, which seems correlated to the smaller lattice parameters (cell volume). From this point of view, the catalytic activity is correlated to both the concentration of anion vacancies and the size/volume of the crystal lattice. In solid state ionics, large lattice parameters will lead bigger cell volume to more 'free volume' (void not occupied by ions), making the migration of anions much easier, leading high ionic conductivity. It has been reported that partially replacing Sm^{3+} ions in $Ce_{0.8}Sm_{0.2}O_{2-\delta}$ with larger Ca^{2+} ions, leads to increased O^{2-} ionic conductivity because of the increased 'free volume', making the migration of O^{2-} much easier [56]. It is expected that the same situation may happen on Sm^{3+} and N^{3-} co-doped CeO_2 , which shares the same crystal structure as $Ce_{0.8}Sm_{0.2}O_{2-\delta}$ (Table 1). This indicates that high mobility of the anions, particularly N^{3-} ions in the oxynitrides, which may participate in the reaction for ammonia synthesis, is another important parameter to achieve high catalytic activity [7]. Theoretically high anion conductivity, particularly N^{3-} ion conductivity, can extend the reaction zone of ammonia synthesis reaction as N^{3-} ions can be formed at anywhere on the surface, then quickly diffuse through the oxynitride particles to an active site. These active sites are the contact

points between α -Fe and $Ce_{1-z}Sm_zO_{2-x}N_y$, and is where the reaction is completed (Fig. 10), leading to higher catalytic activity. Introduction of O^{2-} ionic conduction in electrodes to facilitate the electrode reaction has been widely used in SOFCs. This key strategy may also be employed to the catalytic reaction for ammonia synthesis to improve the activity of composite catalysts if anions such as N^{3-} ions also take part in the reaction.

3.6. Comparison of Fe catalyst promoted by CeO_2 , $CeO_{2-x}N_y$ and $Ce_{0.5}Sm_{0.5}O_{2-x}N_y$

The anion vacancy promotion effect due to the doping of nitrogen in CeO_2 , CeO_2 mixed with the Fe-catalyst at the same mass ratio (20 : 80) was also investigated, as shown in Fig. 8a&b. In the measured temperature range, Fe- $CeO_{2-x}N_y$ shows much higher activity than Fe- CeO_2 , indicating the vacancy-rich $CeO_{2-x}N_y$ is a better promoter. At 3 MPa and 450 °C, the ammonia formation rate increases from 9.7 $\text{mmol g}^{-1} \text{ h}^{-1}$ to 17.2 $\text{mmol g}^{-1} \text{ h}^{-1}$ when Fe- CeO_2 is replaced with Fe- $CeO_{2-x}N_y$, almost doubling the activity. This provides further evidence that the anion vacancies, particularly nitrogen vacancies, may take part in the reaction, leading to increased activity [7,22,26,27]. The slightly increased activity of the Fe- CeO_2 catalyst at 600 °C and 3 MPa (Fig. 3b) could be related to the formation of intrinsic oxygen vacancies at high temperature with the presence of high pressure H_2 (Eq. (2)). The maximum rate allowed at our reactor conditions according to thermodynamic equilibrium is shown in Fig. 8a & b [54]. It can be seen that for both 1 MPa and 3 MPa, the reactions approach the equilibrium conversion as temperature increases. For both pressures, the catalyst reaches their peak activity at values lower than the thermodynamic equilibrium rate.

The apparent activation energies of the Fe catalysts promoted by all three promoters are lower than 70 kJ/mol for the representative industrial Fe catalyst (Fig. 8c & d) [5,52]. The activation energies for Fe- CeO_2 and Fe- $CeO_{2-x}N_y$ are around 60 kJ mol^{-1} , slightly higher than that for Fe- $Ce_{0.5}Sm_{0.5}O_{2-x}N_y$ (Fig. 6e). The presence of a large amount of anion vacancies in $Ce_{0.5}Sm_{0.5}O_{2-x}N_y$ benefits the ammonia synthesis reaction, reducing the apparent activation energy (Table 1).

3.7. Relationship between ammonia synthesis rate and space velocities

The ammonia synthesis rate is a key parameter when people talk about the activity of a catalyst. The ammonia synthesis rate is related to the activity of the catalyst, the loading of the catalyst and gas flow rate (space velocity). The effect of space velocity on the ammonia synthesis rate and conversion of 80 wt%Fe-20 wt% $Ce_{0.5}Sm_{0.5}O_{2-x}N_y$ at 400 °C, 3 MPa is shown in Figure S7. The rate of formed ammonia increased as

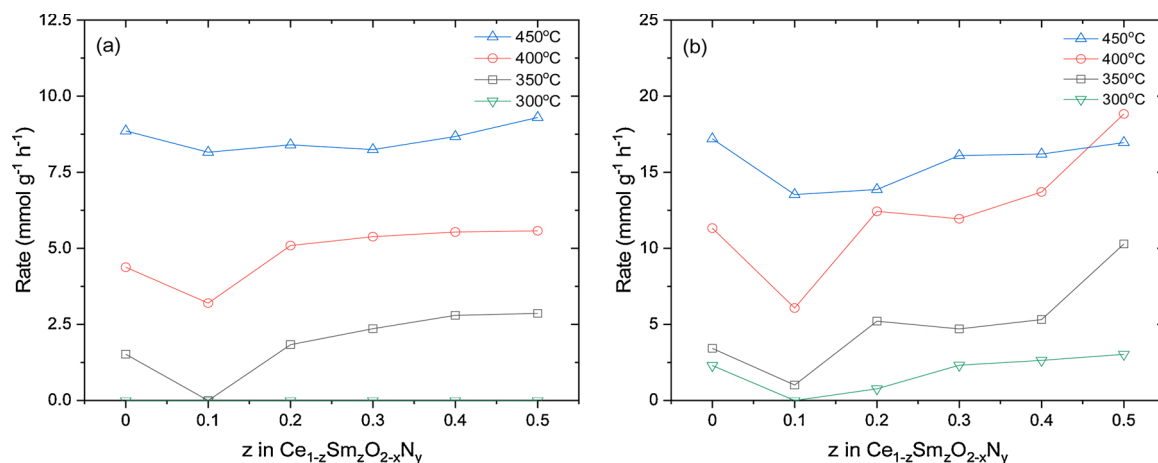


Fig. 7. (a) The ammonia synthesis rate as the level of samarium dopant is increased in the $Ce_{1-z}Sm_zO_{2-x}N_y$ promoter at 1 MPa; (b) The ammonia synthesis rate as the level of samarium dopant is increased in the $Ce_{1-z}Sm_zO_{2-x}N_y$ promoter at 3 MPa.

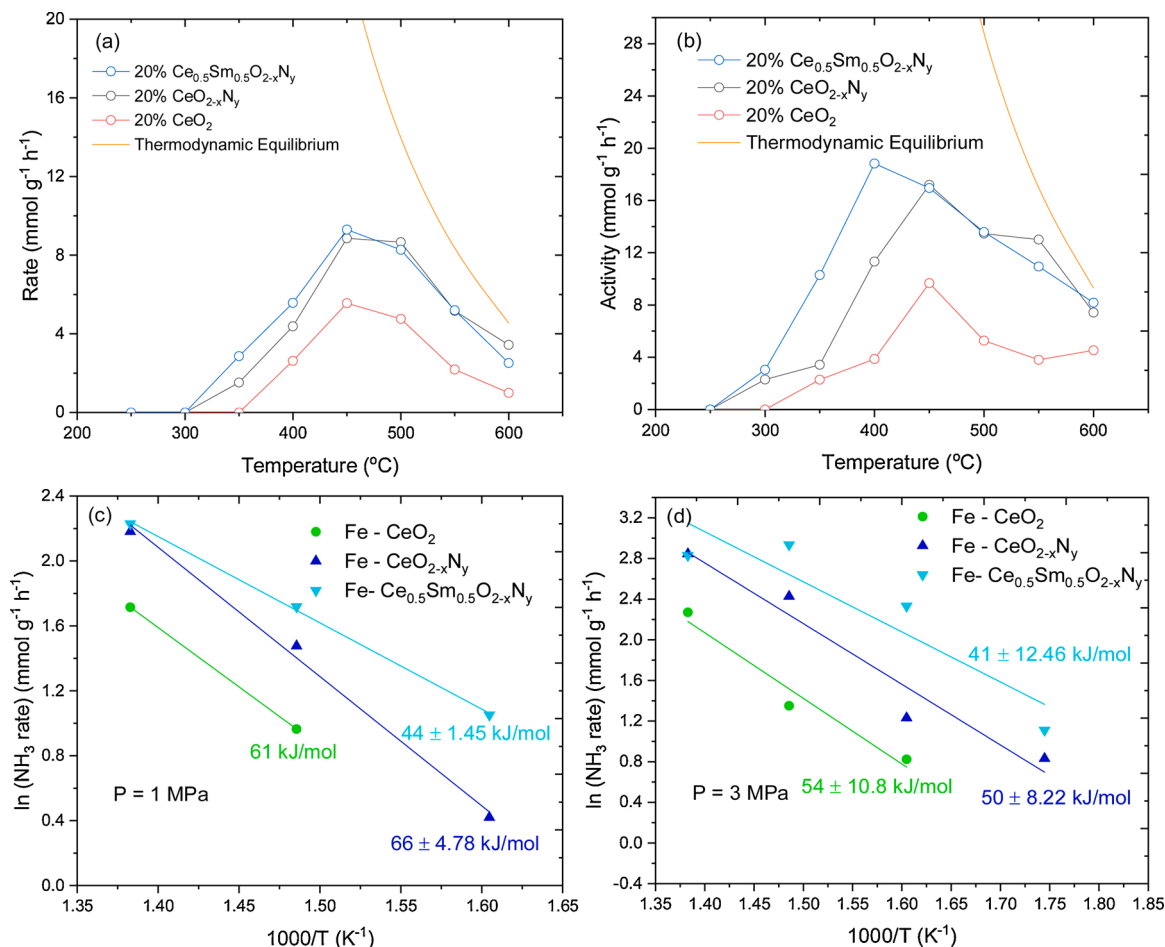


Fig. 8. (a) The ammonia synthesis rates of 80 % Fe – 20 % CeO₂, 80 % Fe – 20 % CeO_{2-x}N_y, 80 % Fe – 20 % Ce_{0.5}Sm_{0.5}O_{2-x}N_y, at different temperatures and 1 MPa, and Thermodynamic Equilibrium at 1 MPa; (b) Ammonia synthesis rates of 80 % Fe – 20 % CeO_{2-x}N_y, 80 % Fe – 20 % Ce_{0.5}Sm_{0.5}O_{2-x}N_y, 80 % Fe – 20 % CeO₂ at different temperatures and 3 MPa, and Thermodynamic Equilibrium at 3 MPa; (c) Arrhenius plots used to find activation energies. Fe-CeO₂, Fe - CeO_{2-x}N_y and Fe-Ce_{0.5}Sm_{0.5}O_{2-x}N_y with 20 wt% promoter 1 MPa; (d) Arrhenius plots used to find activation energies. Fe-CeO₂, Fe - CeO_{2-x}N_y and Fe-Ce_{0.5}Sm_{0.5}O_{2-x}N_y with 20 wt% promoter 3 MPa.

flow rate of the feed gases and WHSV was increased. However, total conversion increases at reduced feed gas flow rates due to the longer residence time of the reactants in the catalyst bed. A nearly linear relationship between total flow rate and outlet conversion was observed indicating good mass transfer properties between that catalyst and reactants. This experiment indicates that the ammonia synthesis rate is linear to the space velocity in the region tested, the ammonia synthesis rate will be doubled if the space velocity is doubled and vice versa. Therefore, WHSV should be taken into account when comparing the ammonia synthesis rate from different sources [22]. In Table S2, the ammonia synthesis rates from different Fe-based catalysts plus the representative Cs-Ru/MgO are listed together alongside their respective WHSV.

3.8. Stability of the 80 wt% Fe - 20 wt% Ce_{0.5}Sm_{0.5}O_{2-x}N_y catalyst

Stability is an important parameter for industrial ammonia synthesis catalysts. Among all the investigated promoters (CeO₂, CeO_{2-x}N_y and Ce_{1-z}Sm_zO_{2-x}N_y), Ce_{0.5}Sm_{0.5}O_{2-x}N_y exhibits the highest promotion effect (or co-catalyst) to the Fe catalyst for ammonia synthesis. Industrial ammonia reactors usually run continuously for long periods of up to years at a time. Long term stability tests of the new catalysts are carried out as it is vital for commercial applications. The stability of the 80 wt% Fe – 20 wt% CeO_{2-x}N_y catalyst was measured for nearly 200 h in Zero grade feed gas, at the optimised conditions, 450 °C and 3 MPa (Fig. 9a).

There is a slight drop in activity over the first 50 h before the catalyst stabilises then remains stable over the rest of the entire test. This slight initial drop in activity is expected to be caused by the change in nitrogen content in the promoter material which needs to be stabilised in mixed N₂ and H₂ at high temperature and high pressure. At high temperature, it is possible that the Ce_{0.5}Sm_{0.5}O_{2-x}N_y is partially oxidised by the oxygenate impurities as nitrogen was not detected by XPS for the 80 wt % Fe – 20 wt% Ce_{0.5}Sm_{0.5}O_{2-x}N_y sample after the catalytic activity at both 1 and 3 MPa to a temperature up to 600 °C (Fig. 2) although the nitrogen content in Fe - Ce_{0.5}Sm_{0.5}O_{2-x}N_y could be too low, beyond the measuring limit for XPS and CHN.

The stability of the 80 % Fe – 20 % Ce_{0.5}Sm_{0.5}O_{2-x}N_y catalyst at 400 °C and 3 MPa was also measured for over 200 h (Fig. 9b). Similar to the CeO_{2-x}N_y promoted Fe-catalyst, an initial slight drop in activity is also observed, remaining stable for the rest of the tested hours. Although the initial drop is at a similar extent to the CeO_{2-x}N_y promoted Fe-catalyst, the drop in activity for 80 % Fe – 20 % Ce_{0.5}Sm_{0.5}O_{2-x}N_y catalyst continues over a longer period of time, about 100 h. Since the operating temperature is 50 °C (400 °C instead of 450 °C) lower, it could therefore take a longer time to stabilise the nitrogen content in the Ce_{0.5}Sm_{0.5}O_{2-x}N_y promoter.

In conventional ammonia synthesis catalysts, low operating temperatures amplify the poisoning effect of impurities causing a more significant problem than at high temperatures [17,18]. The stability of 80 % Fe – 20 % Ce_{0.5}Sm_{0.5}O_{2-x}N_y catalyst at 300 °C, 3 MPa was therefore

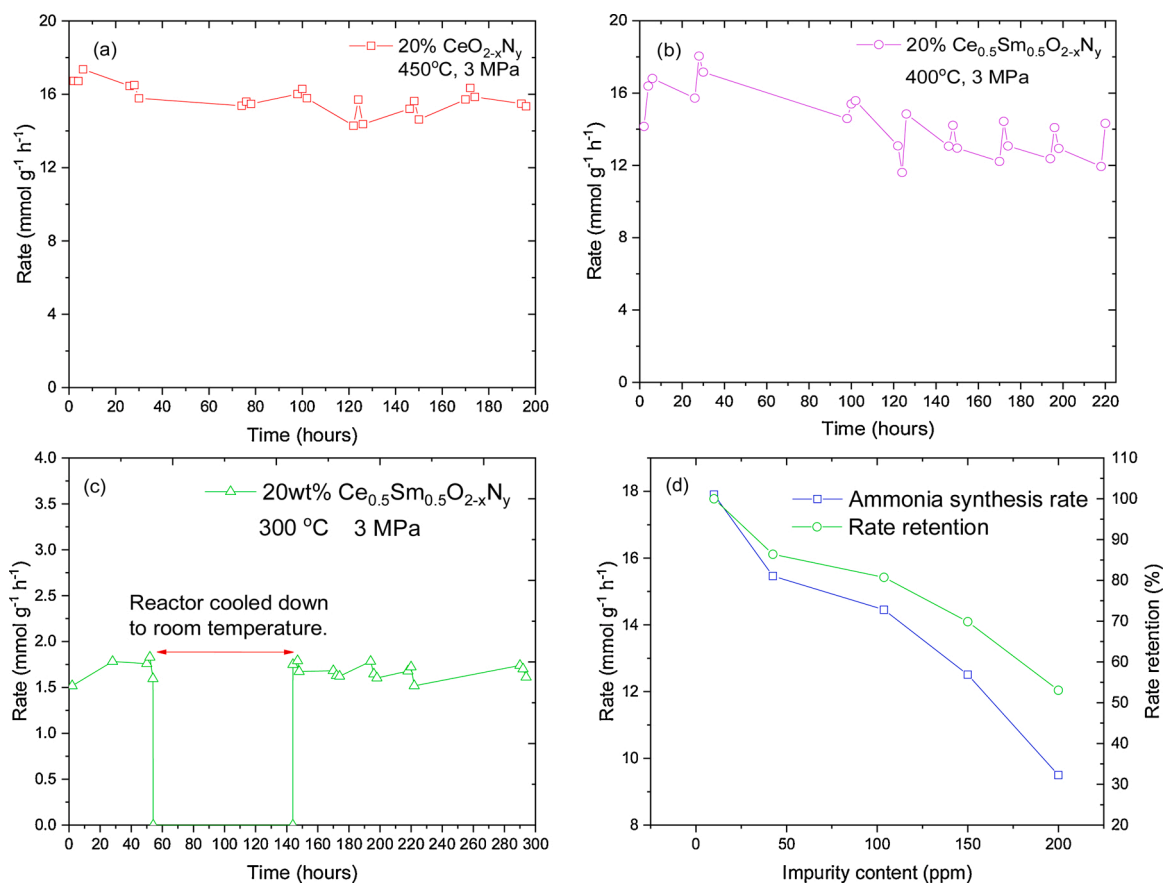


Fig. 9. (a) Activity of the 80 % Fe – 20 % CeO_{2-x}N_y catalyst on stream for over 200 h. A temperature and pressure of 450 °C and 3 MPa respectively were constantly held. (b) Activity of the 80 % Fe – 20 % Ce_{0.5}Sm_{0.5}O_{2-x}N_y catalyst on stream for over 200 h. A temperature and pressure of 400 °C and 3 MPa respectively were constantly held. (c) Activity of the 80 % Fe – 20 % Ce_{0.5}Sm_{0.5}O_{2-x}N_y catalyst on stream for over 200 h. A temperature and pressure of 300 °C and 3 MPa respectively were constantly held. During the measurement, the reactor was cooled down to room temperature without flowing gases and kept at room temperature for ~ 90 h then heated up to 300 °C again. A constant mole ratio of 3 to 1 for H₂ to N₂ respectively was used for the feed gas. Gas flowrate was 80 mL min⁻¹ at daytime and decreased to 40 mL min⁻¹ at night. (d) Ammonia synthesis rates of the 80 %Fe - 20 % Ce_{0.5}Sm_{0.5}O_{2-x}N_y catalyst in gases with oxygenate impurity levels 10 to 200 ppm, 475 °C, 3 MPa and 80 mL min⁻¹ feed gas (H₂/N₂ = 3/1).

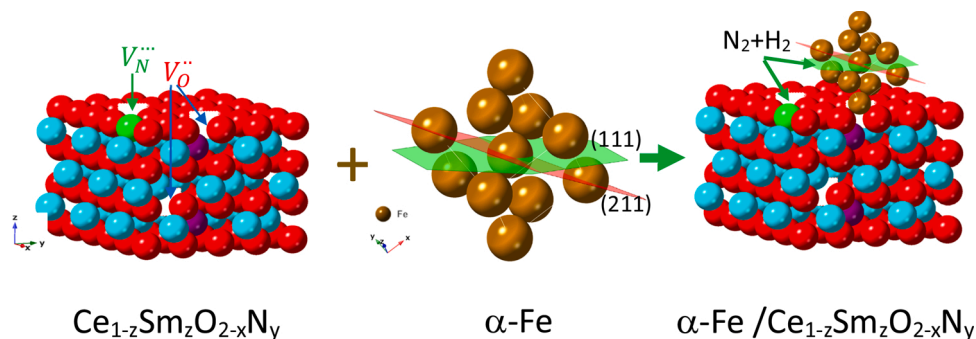


Fig. 10. Schematic diagram on the anion vacancies and their interaction with α -Fe particles and the reactants, H₂ and N₂. The (111) and (211) planes in α -Fe is shown in green and red respectively.

also investigated. This catalyst is stable at 300 °C during the measured 290 h in which there is a ~ 90 h break (Fig. 9c). During the break, the gas flow was stopped, the reactor was cooled down to room temperature with 3 MPa mixed N₂ and H₂ together with the generated NH₃. This experiment indicates that, the oxynitride promoted Fe catalyst exhibits excellent stability in Zero grade feed gas, even at room temperature. This is very different from the conventional industrial fused Fe catalyst as the promoters we used are vastly different. In fused Fe catalysts, the stability relied on the homogeneously distributed Al₂O₃ additive [17,18]. In our

catalyst, there is no added Al₂O₃ at all. The stability of our Fe-oxynitride composite catalysts relied on the SMSI between iron and oxynitride, prohibiting the growth or sintering of the iron particles. Therefore, our Fe-oxynitride catalyst is even more stable at temperatures as low as room temperature [22].

Intermittent operation of the ammonia synthesis reactor is therefore possible as the catalyst will not be damaged during the heating/cooling process. This is particular useful for green ammonia production at a small scale using the surplus intermittent renewable electricity as the

energy sources [2]. The dominant technology for ammonia production will be the Haber-Bosch reaction for the foreseeable future, including green ammonia production [2,18,57]. It has been reported that improving the efficiency of water electrolyser and/or developing new catalysts enabling the agile operation of the Haber-Bosch process are the keys to achieving green ammonia industry [58]. From this point of view, if our cation doped cerium oxynitride promoted catalysts are used in the localised green ammonia synthesis plants, then there is potential for this technology to be used for renewable electricity storage providing a better match with the intermittent nature of the renewable resources. During the stability test at 300 °C, no initial activity drop was observed indicating the nitrogen content is fairly stable at this temperature, which implies $\text{Ce}_{0.5}\text{Sm}_{0.5}\text{O}_{2-x}\text{N}_y$ is not (partially) oxidised by the oxygenate impurity at 300 °C.

It has been reported that high pressures can help to prevent the decomposition of oxynitrides to oxides and nitrogen, and high pressures facilitate the oxynitride synthesis process [59]. Therefore at 3 MPa both $\text{Ce}_{0.5}\text{Sm}_{0.5}\text{O}_{2-x}\text{N}_y$ and $\text{CeO}_{2-x}\text{N}_y$ promoters are expected to have a higher tolerance to decomposition caused by oxygenate impurities in the feeding gas. We tried to test the nitrogen content in the 80 wt%Fe-20 wt % $\text{Ce}_{0.5}\text{Sm}_{0.5}\text{O}_{2-x}\text{N}_y$ catalyst after the stability test, however, due to the large Fe content of 80 wt%, the nitrogen content is too low, beyond the measurement limit of the XPS and CHN facility as the total nitrogen in the total composite catalyst is too small. The stability of oxynitrides is related to both the oxygenate concentration and reaction temperature. When the reaction temperature is reduced to 300 °C, it was found that the catalytic activity of $\text{Fe-Ce}_{0.5}\text{Sm}_{0.5}\text{O}_{2-x}\text{N}_y$ catalyst is stable, indicating that the $\text{Ce}_{0.5}\text{Sm}_{0.5}\text{O}_{2-x}\text{N}_y$ is stable in the less pure feed gas at 300 °C. It has been reported that the Ni-LaN catalyst is stable for ammonia synthesis when ultrapure feed gas (purity > 99.99995 %) was applied [27]. $\text{Ce}_{0.5}\text{Sm}_{0.5}\text{O}_{2-x}\text{N}_y$ could also be chemically stable at higher temperatures when ultrapure feed gas is used for ammonia synthesis.

3.9. Tolerance to oxygenate-containing impurity of the Fe-oxynitride catalysts

It has been confirmed that the 80 % Fe – 20 % $\text{Ce}_{0.5}\text{Sm}_{0.5}\text{O}_{2-x}\text{N}_y$ catalyst exhibits the highest activity without further purification of the Zero grade H_2 and N_2 feed gases. In the past, catalyst tolerance towards impurity is normally tested at fixed concentration of O_2 such as 5 ppm of an oxygenic compound [20], 1 ppm impurity [19,21]. In order to test the limit of our Fluorite oxynitride promoted Fe catalyst, a much higher concentration of impurities was used. The activities of our 80 wt% Fe – 20 wt% $\text{Ce}_{0.5}\text{Sm}_{0.5}\text{O}_{2-x}\text{N}_y$ catalyst at 475 °C and 3 MPa with different impurity levels up to 200 ppm were investigated (Fig. 9d). Here the temperature is the measured temperature of the tube furnace hot zone. This investigation into oxygenate tolerance to 200 ppm impurity was conducted in a newly designed reactor capable of achieving higher pressures with a large wall thickness (0.125 inch instead of 0.083 inch). Due to the less effective heat transfer between the thick wall reactor and hot zone of the furnace, the real temperature of the catalyst in new thick wall reactor is slightly lower [22]. An impurity of 10 ppm in the gas is expected to remain as the O_2 and H_2O traps cannot remove impurities such as CO, CO_2 , and hydrocarbons [22]. To achieve higher impurity levels, zero grade nitrogen was mixed with nitrogen with 1000 ppm O_2 to reach higher quantifiable oxygenate concentrations desired. The activity of the 80 wt% Fe - 20 wt% $\text{Ce}_{0.5}\text{Sm}_{0.5}\text{O}_{2-x}\text{N}_y$ composite catalyst in Zero grade gas is about 86 % of that after the purification process indicating that the oxygenate impurities still exhibit an effect on activity. Higher activity can be obtained if very pure feed gas is applied in our Fe-oxynitride catalysts. Further increases in the total impurity level to 104 ppm, with known injected 61 ppm oxygen, provides a rate retention of 81 %. Please note 61 ppm oxygen equals to 122 ppm atomic oxygen. This is over 10 times of the maximum allowed oxygenate level (10 atomic oxygen) for industrial fused Fe catalysts [17]. The ammonia formation rate is still more than half (53 %) of the original rate in

purified gas when total impurity level was 200 ppm with known injected 158 ppm O_2 . This experiment indicates the 80 wt% Fe – 20 wt% $\text{Ce}_{0.5}\text{Sm}_{0.5}\text{O}_{2-x}\text{N}_y$ composite catalyst exhibits excellent oxygenate tolerance properties. When a feed gas with 200 ppm impurities is used, by doubling the amount of catalyst / the size of the reactor, the same amount of ammonia can be produced compared to standard feed gas with 10 ppm atomic oxygenate. If an oxygenate tolerant catalyst, such as Fe – $\text{Ce}_{1-z}\text{Sm}_z\text{O}_{2-x}\text{N}_y$ composite is used in the reactor, purification requirements will be lower thus saving on initial facility cost and continued energy inputs significantly improving the overall efficiency for ammonia synthesis. However, there is a risk that the oxynitride may be partially oxidised by oxygenate impurities if their concentration is too high at high reaction temperature. The formed Sm-doped CeO_2 will still exhibit high activity and stability but the activity will be slightly lower due to the loss of nitrogen vacancies (Fig. 9b) [22]. Therefore, if we want to take advantage of nitrogen vacancies in $\text{Ce}_{1-z}\text{Sm}_z\text{O}_{2-x}\text{N}_y$ to achieve the high activity it is required to minimise the oxygenate concentration. Developing more stable promoters with anion vacancies present in a high concentration, particularly nitrogen vacancies is therefore desired in order to achieve a high stability in oxygenates.

4. Discussion

The results presented above clearly show that the introduction of a large amount of anion vacancies in CeO_2 through cation (Sm^{3+} ions) and anion (N^{3-} ions) co-doping result in various changes in catalytic properties when used as support for low-cost Fe catalysts for ammonia synthesis. Both stability and activity of the $\text{Fe-Ce}_{1-z}\text{Sm}_z\text{O}_{2-x}\text{N}_y$ composite have been significantly improved, which is attributed to the anion vacancies, particularly nitrogen vacancies. The schematic diagram on the interaction between anion vacancies and α -Fe particles and the reactants, H_2 and N_2 for ammonia synthesis is shown in Fig. 10.

As for the reaction mechanism of oxynitride or oxynitride hydride promoted transition metal (TM) catalysts, Kobayashi et al. reported that oxyhydride $\text{BaTiO}_{3-x}\text{H}_x$ improves the activity of the transition metal catalysts through the oxynitride-hydride intermediate, where both lattice N^{3-} ions and H^- ions play important roles for the increased catalytic activity [5]. Kitano et al. proposed two possible reaction mechanisms for ammonia synthesis over TM / $\text{BaCeO}_{3-x}\text{N}_y\text{H}_z$ catalysts. Both are related to Mars – van Krevelen mechanism through anion vacancies with the participation of lattice N^{3-} and H^- ions [7]. The key evidence for the Mars – van Krevelen mechanism is the low apparent activation energy, 46–62 kJ/mol for TM/ $\text{BaCeO}_{3-x}\text{N}_y\text{H}_z$ catalysts [7]. The introduction of N^{3-} ions to the $\text{BaTiO}_{3-x}\text{H}_x$ lattice through an in situ formed oxynitride-hydride intermediate or, to the perovskite oxynitride hydride $\text{BaCeO}_{3-x}\text{N}_y\text{H}_z$ lattice at the very beginning, will generate anion vacancies from the charge balance. The more N^{3-} ions are introduced into the lattice, the more anion vacancies will be generated. In our $\text{Ce}_{1-z}\text{Sm}_z\text{O}_{2-x}\text{N}_y$, there are N^{3-} ions in the lattice already, similar to $\text{BaCeO}_{3-x}\text{N}_y\text{H}_z$. As for the H^- ions, it has been widely reported that Ce-H species may be formed when CeO_2 is exposed in H_2 at high temperature while more Ce-H species can be formed when more oxygen vacancies are presented in the CeO_2 lattice [60,61]. It is reasonably deduced that, under the ammonia synthesis conditions, in the presence of high concentration (~ 75 %) H_2 at high temperature, some hydride intermediates may also be formed in our cerium oxynitrides. Following this our oxynitride would be a kind of oxynitride hydride, similar to $\text{BaCeO}_{3-x}\text{N}_y\text{H}_z$, although exhibiting a fluorite structure instead of a perovskite structure. The apparent activation energy of the 80 wt% Fe-20 wt% $\text{Ce}_{1-z}\text{Sm}_z\text{O}_{2-x}\text{N}_y$ catalysts with $z \geq 0.3$ is around 45 kJ/mol, which is fairly close to that for the TM/ $\text{BaCeO}_{3-x}\text{N}_y\text{H}_z$ catalysts [7]. The low activation energy plus the presence of N^{3-} ions and possible indirectly formed H^- ions through the intermediate in $\text{Ce}_{1-z}\text{Sm}_z\text{O}_{2-x}\text{N}_y$, are very similar to the case for $\text{BaCeO}_{3-x}\text{N}_y\text{H}_z$, thus they may share the same or similar reaction mechanism.

Another important finding in this study is, the catalytic activity

seems related to the lattice parameter of the $Ce_{1-z}Sm_zO_{2-x}N_y$ support. The larger the lattice volume with larger ‘free volume’, the higher the catalytic activity (Figs. 3b & 7). This can be considered in two aspects: (a) The size of anion vacancies. As shown in Fig. 10, both N_2 and H_2 may be adsorbed on the anion vacancies on the surface. It is believed that the bigger the vacancy (charged void), the easier for the adsorption of N_2/H_2 gases, thus the higher the catalytic activity. (b) The mobility of N^{3-} and H^- ions. When N_2 and H_2 are adsorbed on anion vacancies on the surface of $Ce_{1-z}Sm_zO_{2-x}N_y$, it may dissociate to form N^{3-} and H^- ions, according to the proposed reaction mechanism of oxynitride hydride [7]. High mobility or ionic conductivity of N^{3-} and H^- ions will allow the reaction between N^{3-} ions and adsorbed H^- species on Fe or, between H^- ions and N species on Fe to happen all over the surface of the composite catalyst, rather than limited to the triple phase (Fe- $Ce_{1-z}Sm_zO_{2-x}N_y$ -gaseous reactants) boundary, similar to the case for the reaction on the anode of a solid oxide fuel cell. This will increase the probability for the formation of ammonia thus result in a higher activity. Large lattice volume means large ‘free volume’ thus the ionic conductivity or mobility of the N^{3-}/H^- ions will be higher, leading to higher catalytic activity [62]. It should be noted that Sm-doped CeO_2 is a well-known O^{2-} ionic conductor with high ionic conductivity and has been used as an electrolyte for SOFCs. It is expected that the ionic conductivity for other anions such as N^{3-} and H^- ions in the $Ce_{1-z}Sm_zO_{2-x}N_y$ will also increase at increased lattice parameters thus larger ‘free volume’ for easy diffusion of ions, facilitating the ammonia synthesis reaction [56].

The high concentration of anion vacancies in $Ce_{1-z}Sm_zO_{2-x}N_y$ will facilitate the nesting/anchoring of Fe particles, resulting in SMSI, which has been described above (Fig. 10). This SMSI can prohibit the sintering of Fe particles even under a strong oxidization environment [22,29]. Therefore, a large amount of anion vacancies in cation doped cerium oxynitride improved both the stability and catalytic activity for ammonia synthesis.

It has been reported that, for cubic Fe, (111) plane is the most active for ammonia synthesis reaction. The second most active plane is (211) when exposed to the reactant gases [63]. If a Fe atom is nested onto a surface anion vacancy via SMSI, where the array of anions (O^{2-} and N^{3-} ions) are, ideally the (111) plane is in parallel or close to parallel to the plane of anion arrays. Therefore, the probability for (111) planes to be exposed to the reactants (H_2 and N_2) is very high, thus can maximize the ammonia production [22]. Theoretically N_2 located away from the α -Fe may also be dissociated by nitrogen vacancies not in contact with Fe, then diffuse through the whole $Ce_{1-z}Sm_zO_{2-x}N_y$ particle, then reach the contact point between α -Fe and $Ce_{1-z}Sm_zO_{2-x}N_y$ to catalyze the ammonia synthesis reaction. From all aspects of the ammonia synthesis reaction, oxynitrides with a large amount of anion vacancies, particularly nitrogen vacancies, will benefit the reaction to improve both activity and stability.

5. Conclusions

Cation doped fluorite oxynitrides, new single phase Sm-doped cerium oxynitrides have been synthesized for the first time. For the high Sm-doped cerium oxynitrides, approximately 16.5 % of the anion positions are not occupied. The introduction of nitrogen to form nitrogen vacancies will have better match to the adsorbed N_2 in terms of size. The optimised composition is 80 wt% Fe – 20 wt% $Ce_{0.5}Sm_{0.5}O_{2-x}N_y$ which showed an activity of $18.8 \text{ mmol g}^{-1} \text{ h}^{-1}$ at 400°C , 3 MPa (WHSV = $16000 \text{ mL g}^{-1} \text{ h}^{-1}$) using 99.996 % H_2 and N_2 as the feed gases, comparable to the industrial fused Fe catalyst at a much higher purity. At 350°C and 1 MPa, the activity is among the highest in all reported non-Ru based catalysts. The apparent activity energy of our Fe- $Ce_{1-z}Sm_zO_{2-x}N_y$ catalysts with $z \geq 0.3$ is in the range of 45 kJ/mol, among the lowest E_a for all reported ammonia synthesis catalysts [5,7,27]. It is believed that the reaction proceeds through the Mars – van Krevelen mechanism mediated by the anion vacancies, similar to perovskite oxynitride hydride $BaCeO_{3-x}N_yH_z$. At 3 MPa and 475°C , the activity

retention of the Fe – 20 wt% $Ce_{0.5}Sm_{0.5}O_{2-x}N_y$ catalyst is 70 % with known injected 107.5 ppm O_2 (150 ppm impurity level). The Fe- $Ce_{0.5}Sm_{0.5}O_{2-x}N_y$ catalyst exhibits excellent stability at 300°C , even after cooling to room temperature implying stability at room temperature. This is suitable for agile operation of localised green ammonia synthesis plants using intermittent energy from renewable electricity. Both catalysts starting from α - Fe_2O_3 - oxynitride are stable in air at room temperature and are thus easy to handle. This article provides a new development strategy for the synthesis of novel oxygenate-tolerant ammonia synthesis catalysts that can be used for both existing large scale Haber-Bosch processes as well as small scale green ammonia synthesis from renewable energy sources. Agile operation is key for small scale ammonia plants utilising intermittent renewable energy, therefore, future work thoroughly investigating the catalyst tolerance to the thermal shock of reactor start-up/shut-down should be investigated based on the promising results highlighted in the stability test. The development of a large weight percent iron based catalyst will have vast cost advantages over expensive Ru and Co based catalysts. However, the replacement of relatively expensive rare earth elements in the oxynitride provides room for further improvements in this regard, which is under investigation.

Declaration of Competing Interest

None.

Acknowledgement

The authors thank EPSRC (Grant No. EP/G01244X/1) for funding.

Appendix A. Supplementary data

Supplementary material related to this article can be found, in the online version, at doi:<https://doi.org/10.1016/j.apcatb.2020.119843>.

References

- [1] J.W. Erisman, M.A. Sutton, J. Galloway, Z. Klimont, W. Winiwarter, How a century of ammonia synthesis changed the world, *Nat. Geosci.* 1 (2008) 636–639.
- [2] R. Lan, J.T.S. Irvine, S.W. Tao, Ammonia and related chemicals as potential indirect hydrogen storage materials, *Int. J. Hydrogen Energy* 37 (2012) 1482–1494.
- [3] Y. Inoue, M. Kitano, S.W. Kim, T. Yokoyama, M. Hara, H. Hosono, Highly Dispersed Ru on Electride $Ca_{24}Al_{28}O_{64}^{4+}(e^-)_4$ as a Catalyst for Ammonia Synthesis, *ACS Catal.* 4 (2014) 674–680.
- [4] M. Kitano, Y. Inoue, M. Sasase, K. Kishida, Y. Kobayashi, K. Nishiyama, T. Tada, S. Kawamura, T. Yokoyama, M. Hara, H. Hosono, Self-organized ruthenium–barium core–shell nanoparticles on a mesoporous calcium amide matrix for efficient low-temperature ammonia synthesis, *Angew. Chemie Int. Ed.* 57 (2018) 2648–2652.
- [5] Y. Tang, Y. Kobayashi, N. Masuda, Y. Uchida, H. Okamoto, T. Kageyama, S. Hosokawa, F. Loyer, K. Mitsuhashi, K. Yamanaoka, Y. Tamenori, C. Tassel, T. Yamamoto, T. Tanaka, H. Kageyama, Metal-dependent support effects of oxyhydride-supported Ru, Fe, Co catalysts for Ammonia synthesis, *Adv. Energy Mater.* 8 (2018) 1801772.
- [6] Y. Kobayashi, Y. Tang, T. Kageyama, H. Yamashita, N. Masuda, S. Hosokawa, H. Kageyama, Titanium-based hydrides as heterogeneous catalysts for Ammonia synthesis, *J. Am. Chem. Soc.* 139 (2017) 18240–18246.
- [7] M. Kitano, J. Kujirai, K. Ogasawara, S. Matsuishi, T. Tada, H. Abe, Y. Niwa, H. Hosono, Low-temperature synthesis of perovskite oxynitride-hydrides as ammonia synthesis catalysts, *J. Am. Chem. Soc.* 141 (2019) 20344–20353.
- [8] X.Y. Wang, X.B. Peng, W. Chen, G.Y. Liu, A.M. Zheng, L.R. Zheng, J. Ni, C.T. Au, L. L. Jiang, Insight into dynamic and steady-state active sites for nitrogen activation to ammonia by cobalt-based catalyst, *Nat. Commun.* 11 (2020) 653.
- [9] B. Cui, Z. Yu, S. Liu, J. Zhang, X. Liu, C. Liu, Z. Zhang, Highly selective and efficient ammonia synthesis from N_2 and H_2O via an iron-based electrolytic-chemical cycle, *Int. J. Hydrogen Energy* 45 (2020) 94–102.
- [10] S. Chen, S. Perathoner, C. Ampelli, H. Wei, S. Abate, B. Zhang, G. Centi, Enhanced performance in the direct electrocatalytic synthesis of ammonia from N_2 and H_2O by an in-situ electrochemical activation of CNT-supported iron oxide nanoparticles, *J. Energy Chem.* 49 (2020) 22–32.
- [11] H. Li, Y. Liu, Y. Liu, L. Wang, R. Tang, P. Deng, Z. Xu, B. Haynes, C. Sun, J. Huang, Efficient visible light driven Ammonia synthesis on sandwich structured $C3N_4/MoS_2/Mn_3O_4$ catalyst, *Appl. Catal. B Environ.* 281 (2021) 119476.

- [12] K. Murakami, Y. Tanaka, R. Sakai, K. Toko, K. Ito, A. Ishikawa, T. Higo, T. Yabe, S. Ogo, M. Ikeda, H. Tsuneki, H. Nakai, Y. Sekine, The important role of N₂H formation energy for low-temperature ammonia synthesis in an electric field, *Catal. Today* 351 (2020) 119–124.
- [13] X. Yao, Z.-W. Chen, Y.-R. Wang, X.-Y. Lang, Y.-F. Zhu, W. Gao, Q. Jiang, High-loading intrinsic active sites for ammonia synthesis using efficient single-atom catalyst: 2D tungsten-porphyrin sheet, *Appl. Surf. Sci.* 529 (2020) 147183.
- [14] P. Wang, F. Chang, W. Gao, J. Guo, G. Wu, T. He, P. Chen, Breaking scaling relations to achieve low-temperature ammonia synthesis through LiH-mediated nitrogen transfer and hydrogenation, *Nat. Chem.* 9 (2016) 64–70.
- [15] W. Gao, J. Guo, P. Chen, Hydrides, amides and imides mediated ammonia synthesis and decomposition, *Chinese J. Chem.* 37 (2019) 442–451.
- [16] Y. Ogura, K. Sato, S.-I. Miyahara, Y. Kawano, T. Toriyama, T. Yamamoto, S. Matsumura, S. Hosokawa, K. Nagaoka, Efficient ammonia synthesis over a Ru/La_{0.5}Ce_{0.5}O_{1.75} catalyst pre-reduced at high temperature, *Chem. Sci.* 9 (2018) 2230–2237.
- [17] H. Liu, *Ammonia Synthesis Catalysts: Innovation and Practice*, World Scientific Publishing Company, 2013.
- [18] B.A. Rohr, A.R. Singh, J.K. Norskov, A theoretical explanation of the effect of oxygen poisoning on industrial Haber-Bosch catalysts, *J. Catal.* 372 (2019) 33–38.
- [19] B. Fastrup, H. Nygård Nielsen, On the influence of oxygen on iron catalysts during ammonia synthesis and catalyst characterization, *Catal. Lett.* 14 (1992) 233–239.
- [20] F. Rosowski, M. Muhler, The influence of oxygen poisoning on a multiply promoted iron catalyst used for ammonia synthesis: a temperature-programmed desorption and reaction study, in: G.F. Froment, K.C. Waugh (Eds.), *Stud. Surf. Sci. Catal.*, Elsevier, 1997, pp. 111–120.
- [21] J. Folke, H. Song, J. Schittkowski, R. Schlögl, H. Ruland, Oxygen poisoning in laboratory testing of iron-based ammonia synthesis catalysts and its potential sources, *Chemie Ingenieur Technik* (2020), <https://doi.org/10.1002/cite.202000100> n/a.
- [22] J. Humphreys, R. Lan, S.G. Chen, S.W. Tao, Improved stability and activity of Fe-based catalysts through strong metal support interactions due to extrinsic oxygen vacancies in Ce_{0.8}Sm_{0.2}O_{2.8} for the efficient synthesis of ammonia, *J. Mater. Chem. A* 8 (2020) 16676–16689.
- [23] J.A. Farmer, C.T. Campbell, Ceria maintains smaller metal catalyst particles by strong metal-support bonding, *Science* 329 (2010) 933–936.
- [24] Y. Ma, G. Lan, W. Fu, Y. Lai, W. Han, H. Tang, H. Liu, Y. Li, Role of surface defects of carbon nanotubes on catalytic performance of barium promoted ruthenium catalyst for ammonia synthesis, *J. Energy Chem.* 41 (2020) 79–86.
- [25] J. Humphreys, R. Lan, D.W. Du, W. Xu, S.W. Tao, Promotion effect of proton-conducting oxide BaZr_{0.1}Ce_{0.7}Y_{0.2}O_{3.8} on the catalytic activity of Ni towards ammonia synthesis from hydrogen and nitrogen, *Int. J. Hydrogen Energy* 43 (2018) 17726–17736.
- [26] J.H. Shanwen W. Tao, Patent application WO2019/207303, 2018.
- [27] T.-N. Ye, S.-W. Park, Y. Lu, J. Li, M. Sasase, M. Kitano, T. Tada, H. Hosono, Vacancy-enabled N₂ activation for ammonia synthesis on an Ni-loaded catalyst, *Nature* 583 (2020) 391–395.
- [28] C. Wagner, Über den mechanismus der elektrischen stromleitung im nernststift, *Naturwissenschaften* 31 (1943) 265–268.
- [29] M.G. Sanchez, J.L. Gazquez, Oxygen vacancy model in strong metal support interaction, *J. Catal.* 104 (1987) 120–135.
- [30] G.I. Siakavelas, N.D. Charisiou, S. Alkhoori, A.A. Alkhoori, V. Sebastian, S. J. Hinder, M.A. Baker, I.V. Yentekakis, K. Polychronopoulou, M.A. Goula, Highly selective and stable nickel catalysts supported on ceria promoted with Sm₂O₃, Pr₂O₃ and MgO for the CO₂ methanation, *Appl. Catal. B Environ.* 282 (2020) 119562.
- [31] A.B. Jorge, Y. Sakatani, C. Boissiere, C. Laberty-Roberts, G. Sauthier, J. Fraxedas, C. Sanchez, A. Fuytes, Nanocrystalline N-doped ceria porous thin films as efficient visible-active photocatalysts, *J. Mater. Chem.* 22 (2012) 3220–3226.
- [32] G. Goula, G. Botzolaki, A. Osatiasthiani, C.M.A. Parlett, G. Kyriakou, R.M. Lambert, I.V. Yentekakis, Oxidative Thermal Sintering and Redispersion of Rh Nanoparticles on Supports with High Oxygen Ion Mobility, *Catalysts* 9 (2019) 541.
- [33] I.V. Yentekakis, G. Goula, P. Panagiotopoulou, S. Kampouri, M.J. Taylor, G. Kyriakou, R.M. Lambert, Stabilization of catalyst particles against sintering on oxide supports with high oxygen ion lability exemplified by Ir-catalyzed decomposition of N₂O, *Appl. Catal. B Environ.* 192 (2016) 357–364.
- [34] I.V. Yentekakis, G. Goula, S. Kampouri, I. Betsi-Argyropoulou, P. Panagiotopoulou, M.J. Taylor, G. Kyriakou, R.M. Lambert, Ir-Catalysed Nitrous oxide (N₂O) Decomposition: Effect of Ir Particle Size and Metal-Support Interactions, *Catal. Lett.* 148 (2018) 341–347.
- [35] A. Trovarelli, Structural and oxygen storage/release properties of CeO₂-based solid solutions, *Comments Inorg. Chem.* 20 (1999) 263–284.
- [36] S. Sengodan, R. Lan, J. Humphreys, D. Du, W. Xu, H. Wang, S.W. Tao, Advances in reforming and partial oxidation of hydrocarbons for hydrogen production and fuel cell applications, *Renew. Sustain. Energy Rev.* 82 (2018) 761–780.
- [37] I.V. Yentekakis, G. Goula, M. Hatzisymeon, I. Betsi-Argyropoulou, G. Botzolaki, K. Kousi, D.I. Kondarides, M.J. Taylor, C.M.A. Parlett, A. Osatiasthiani, G. Kyriakou, J.P. Holgado, R.M. Lambert, Effect of support oxygen storage capacity on the catalytic performance of Rh nanoparticles for CO₂ reforming of methane, *Appl. Catal. B Environ.* 243 (2019) 490–501.
- [38] G. Botzolaki, G. Goula, A. Rontogianni, E. Nikolarakaki, N. Chalmes, P. Zygouri, M. Karakassides, D. Gournis, N. Charisiou, M. Goula, S. Papadopoulos, I. Yentekakis, CO₂ methanation on supported Rh nanoparticles: the combined effect of support oxygen storage capacity and Rh particle size, *Catalysts* 10 (2020) 944.
- [39] R.D. Shannon, Reised effective ionic-radii and systematic studies of interatomic distances in halides and chalcogenides, *Acta Crystallogr. Sect. A* 32 (1976) 751–767.
- [40] A. Singhanian, S.M. Gupta, CeO_{2-x}N_x solid solutions: synthesis, characterization, electronic structure and catalytic study for CO oxidation, *Catal. Lett.* 148 (2018) 2001–2007.
- [41] K. Eguchi, T. Setoguchi, T. Inoue, H. Arai, Electrical-properties of ceria-based oxides and their application to solid oxide fuel cells, *Solid State Ion.* 52 (1992) 165–172.
- [42] S. Al Sobhi, J.S.J. Hargreaves, A.L. Hector, S. Laassiri, Citrate-gel preparation and ammonia synthesis activity of compounds in the quaternary (Ni,M)₂Mo₃N (M = Cu or Fe) systems, *Dalton Trans.* 48 (2019) 16786–16792.
- [43] B.H. Toby, EXPGUI, a graphical user interface for GSAS, *J. Appl. Crystallogr.* 34 (2001) 210–213.
- [44] A.C. Larson, R.B. Von Dreele, General Structure Analysis System (GSAS), General Structure Analysis System (GSAS), Los Alamos National Laboratory Report, LAUR-86, 2004.
- [45] M. Wolcyz, L. Kepinski, Rietveld refinement of the structure of CeOCl formed in Pd/CeO₂ catalyst - notes on the existence of a stabilized tetragonal phase of La₂O₃ in La-Pd-O system, *J. Solid State Chem.* 99 (1992) 409–413.
- [46] H. Inaba, H. Tagawa, Ceria-based solid electrolytes, *Solid State Ion.* 83 (1996) 1–16.
- [47] M. Yashima, S. Kobayashi, Positional disorder of oxygen ions in ceria at high temperatures, *Appl. Phys. Lett.* 84 (2004) 526–528.
- [48] A. Fuytes, Chemistry and applications of oxynitride perovskites, *J. Mater. Chem.* 22 (2012) 3293–3299.
- [49] M. Guo, J. Lu, Y. Wu, Y. Wang, M. Luo, UV and visible Raman studies of oxygen vacancies in rare-earth-doped ceria, *Langmuir* 27 (2011) 3872–3877.
- [50] M.-F. Luo, Z.-L. Yan, L.-Y. Jin, M. He, Raman spectroscopic study on the structure in the surface and the bulk shell of Ce_xPr_{1-x}O_{2.8} mixed oxides, *J. Phys. Chem. B* 110 (2006) 13068–13071.
- [51] C.D. Zeinalipour-Yazdi, J.S.J. Hargreaves, C.R.A. Catlow, Nitrogen activation in a mars-van krevelen mechanism for Ammonia synthesis on Co₃Mo₃N, *J. Phys. Chem. C* 119 (2015) 28368–28376.
- [52] S. Hagen, R. Barfod, R. Fehrmann, C.J.H. Jacobsen, H.T. Teunissen, I. Chorkendorff, Ammonia synthesis with barium-promoted iron-cobalt alloys supported on carbon, *J. Catal.* 214 (2003) 327–335.
- [53] M. Kitano, Y. Inoue, Y. Yamazaki, F. Hayashi, S. Kanbara, S. Matsuishi, T. Yokoyama, S.-W. Kim, M. Hara, H. Hosono, Ammonia synthesis using a stable electrode as an electron donor and reversible hydrogen store, *Nat. Chem.* 4 (2012) 934–940.
- [54] F. Haber, The synthesis of ammonia from its elements Nobel Lecture, June 2, 1920, *Resonance* 7 (2002) 86–94.
- [55] Z. Lendzion-Bielun, R. Pelka, W. Arabczyk, Study of the kinetics of Ammonia synthesis and decomposition on Iron and cobalt catalysts, *Catal. Lett.* 129 (2009) 119–123.
- [56] S. Banerjee, P.S. Devi, D. Topwal, S. Mandal, K. Menon, Enhanced ionic conductivity in Ce_{0.8}Sm_{0.2}O_{1.9}: unique effect of calcium co-doping, *Adv. Funct. Mater.* 17 (2007) 2847–2854.
- [57] D.R. MacFarlane, P.V. Cherepanov, J. Choi, B.H.R. Suryanto, R.Y. Hodgetts, J. M. Bakker, F.M. Ferrero Vallana, A.N. Simonov, A roadmap to the Ammonia economy, *Joule* 4 (2020) 1186–1205.
- [58] C. Smith, A.K. Hill, L. Torrente-Murciano, Current and future role of Haber-bosch ammonia in a carbon-free energy landscape, *Energy Environ. Sci.* 13 (2020) 331–344.
- [59] A. Fuytes, Synthetic approaches in oxynitride chemistry, *Prog. Solid State Chem.* 51 (2018) 63–70.
- [60] Z.L. Wu, Y.Q. Cheng, F. Tao, L. Daemen, G.S. Foo, L. Nguyen, X.Y. Zhang, A. Beste, A.J. Ramirez-Cuesta, Direct neutron spectroscopy observation of cerium hydride species on a cerium oxide catalyst, *J. Am. Chem. Soc.* 139 (2017) 9721–9727.
- [61] Z.R. Li, K. Werner, K. Qian, R. You, A. Plucienik, A. Jia, L.H. Wu, L.Y. Zhang, H. B. Pan, H. Kuhlbeck, S. Shaikhtudinov, W.X. Huang, H.J. Freund, Oxidation of reduced ceria by incorporation of hydrogen, *Angew. Chemie Int. Ed.* 58 (2019) 14686–14693.
- [62] M.C. Verbraeken, C. Cheung, E. Suard, J.T.S. Irvine, High H⁻ ionic conductivity in barium hydride, *Nat. Mater.* 14 (2015) 95–100.
- [63] D. Strongin, S. Bare, G. Somorjai, The effects of aluminum oxide in restructuring iron single crystal surfaces for ammonia synthesis, *J. Catal.* 103 (1987) 289–301.